ORIGINAL PAPER



Toward accurate density and interfacial tension modeling for carbon dioxide/water mixtures

Zixuan Cui¹ · Huazhou Li¹

Received: 4 July 2020 / Accepted: 13 October 2020 © The Author(s) 2020

Abstract

Phase behavior of carbon dioxide/water binary mixtures plays an important role in various CO₂-based industry processes. This work aims to screen a thermodynamic model out of a number of promising candidate models to capture the vapor–liquid equilibria, liquid–liquid equilibria, and phase densities of CO₂/H₂O mixtures. A comprehensive analysis reveals that Peng–Robinson equation of state (PR EOS) (Peng and Robinson 1976), Twu α function (Twu et al. 1991), Huron–Vidal mixing rule (Huron and Vidal 1979), and Abudour et al. (2013) volume translation model (Abudour et al. 2013) is the best model among the ones examined; it yields average absolute percentage errors of 5.49% and 2.90% in reproducing the experimental phase composition data and density data collected in the literature. After achieving the reliable modeling of phase compositions and densities, a new IFT correlation based on the aforementioned PR EOS model is proposed through a nonlinear regression of the measured IFT data collected from the literature over 278.15–477.59 K and 1.00–1200.96 bar. Although the newly proposed IFT correlation only slightly improves the prediction accuracy yielded by the refitted Chen and Yang (2019)'s correlation (Chen and Yang 2019), the proposed correlation avoids the inconsistent predictions present in Chen and Yang (2019)'s correlation and yields smooth IFT predictions.

Keywords Phase behavior · CO₂/H₂O binary mixtures · Volume translation · Interfacial tension

1 Introduction

The interaction of CO_2 with H_2O is frequently seen in several subterranean processes (such as CO_2 -based enhanced recovery and CO_2 storage). Phase behavior of CO_2/H_2O mixtures under subterranean conditions plays a great role in affecting the overall efficiency of these processes. Thus how to accurately model the phase behavior of CO_2/H_2O mixtures becomes drastically important. Overall, an appropriate combination of cubic equation of state (CEOS), mixing rule in CEOS, α function, volume translation, and interfacial tension (IFT) model should be determined to well capture the vapor–liquid equilibrium (VLE), liquid–liquid equilibrium (LLE), phase density, and IFT of CO_2/H_2O mixtures.

Edited by Yan-Hua Sun

Published online: 19 November 2020

Due to their simplicity and good reliability, CEOSs such as SRK EOS (Soave 1972) and PR EOS (Peng and Robinson 1976) are the most widely used thermodynamic models for the phase behavior modeling of CO₂/H₂O binary mixtures (Aasen et al. 2017; Michelsen and Mollerup 2007). Numerous articles have addressed phase-composition modeling of CO_2/H_2O mixtures. Two types of methods, $\phi-\phi$ (fugacity–fugacity) approach and γ – ϕ (activity–fugacity) approach (Trusler 2017; Zhao and Lvov 2016), are often applied in such modeling processes. Because γ - ϕ approach has a discontinuity issue in the phase diagram near the critical region (Zhao and Lvov 2016), this work focuses on ϕ - ϕ based methods. Valtz et al. (2004) found that the most accurate model is PR EOS (Peng and Robinson 1976), Mathias-Copeman α function (Mathias and Copeman 1983), and Wong-Sandler mixing rule (Wong and Sandler 1992) with average absolute percentage deviation (AAD) of 5.4% in reproducing the measured phase composition data for CO₂/H₂O mixtures. However, the temperature and pressure ranges used by Valtz et al. (2004) were narrow (278.2-318.2 K and 4.64-79.63 bar, respectively). In addition, the parameters in the Wong-Sandler mixing rule



Department of Civil and Environmental Engineering, School of Mining and Petroleum Engineering, University of Alberta, Edmonton, AB T6G 1H9, Canada

(Wong and Sandler 1992) are given as discrete values at different isotherms. Zhao and Lvov (2016) applied PRSV EOS (Stryjek and Vera 1986) and the Wong-Sandler mixing rule to calculate phase compositions, obtaining an AAD of 7.12% in reproducing the measured phase composition data of CO₂/H₂O mixtures over a wide range of temperatures and pressures. Similar to Valtz et al. (2004)'s study, in the study by Zhao and Lvov (2016), the parameters in the Wong-Sandler mixing rule are provided as discrete values at different isotherms, instead of generalized correlations; their model is inconvenient to use since one has to make extrapolations based on the provided values when making predictions at conditions different from those given by Zhao and Lvov (2016). Abudour et al. (2012a) applied van der Waals (1873) one-fluid (vdW) mixing rule with several temperature-dependent BIP correlations in PR EOS in determining phase compositions of CO₂/H₂O mixtures. With the tuned BIPs, their model yielded good accuracy (i.e., AAD of 5.0%) in aqueous phase-composition predictions but lower accuracy (i.e., AAD of 13.0%) in CO₂-rich phase-composition predictions, respectively.

A recent comprehensive study by Aasen et al. (2017) revealed that the most accurate thermodynamic model (among the ones examined by them) in phase-composition and phase-density predictions for $\mathrm{CO_2/H_2O}$ mixtures is PR EOS, Twu α function (Twu et al. 1991), Huron-Vidal mixing rule, and constant volume translation. This model only yields an AAD of 4.5% in phase-composition calculations and an AAD of 2.8% in phase-density calculations for $\mathrm{CO_2/H_2O}$ mixtures. Aasen et al. (2017), Valtz et al. (2004), and Zhao and Lvov (2016) also pointed out that more advanced models [e.g., the Cubic-Plus-Association (CPA) EOS (Kontogeorgis et al. 1996)] do not guarantee an improvement in the phase-composition predictions for $\mathrm{CO_2/H_2O}$ mixtures.

With regards to phase-density calculations, CEOS based methods tend to overestimate liquid-phase molar volumes. A detailed discussion of this issue can be found in the studies by Matheis et al. (2016) and Young et al. (2017). In order to address this problem, Martin (1979) introduced the volume translation concept in CEOS to improve liquid-phase volumetric predictions. Peneloux et al. (1982) developed volume translation schemes in SRK EOS for pure substances. Jhaveri and Youngren (1988) applied volume translation into PR EOS, leading to the improvement of liquid phasedensity predictions. A thorough comparison of different types of volume translation methods can be found in Young et al. (2017)'s work. According to the study by Young et al. (2017), the temperature-dependent volume translation method developed by Abudour et al. (2012b, 2013) provides the most accurate estimates on liquid-phase densities without thermodynamic inconsistencies (e.g., crossover of pressure-volume isotherms). Aasen et al. (2017) applied constant volume translation to phase-density calculations

of CO₂/H₂O mixtures and achieved a significant improvement in density-prediction accuracies. However, a more accurate volume translation function, the one proposed by Abudour et al. (2012b, 2013), was not applied in Aasen et al. (2017)'s study; furthermore, it should be noted that Aasen et al. (2017) used GERG-2008 (Kunz and Wagner 2012) and EOS-CG (Gernert and Span 2016) calculated densities as reference densities instead of experimental data. In this study, we apply the volume translation method by Abudour et al. (2012b, 2013) to see if the use of this model can further improve phase-density predictions for CO₂/H₂O mixtures; these predictions are compared to the measured density data documented in the literature.

Parachor model (Sugden 1930) is one of the most widely applied models in predicting mixtures' IFT (Schechter and Guo 1998). However, its accuracy heavily relies on the density difference between the two coexisting phases in a VLE or an LLE. Our experience in using Parachor model to calculate IFT of CO₂/H₂O mixtures shows that Parachor model is generally appropriate for the IFT estimation for VLE of CO₂/H₂O systems, but less suitable for the IFT estimation for LLE of CO₂/H₂O systems. This is primarily because an LLE of a CO₂/H₂O mixture has a smaller density difference than a VLE. Several empirical IFT correlations for CO₂/ H₂O mixtures have been proposed in the literature. However, most of these correlations are only applicable to a limited temperature and pressure range (Zhang et al. 2016). Hebach et al. (2002) proposed a new correlation which correlated IFT with phase densities. Hebach et al. (2002)'s model is suitable over a wide range of temperature and pressure conditions, although the prediction accuracy decreases with an increase in temperature or pressure. Chen and Yang (2019) proposed a new empirical IFT correlation for CO₂/CH₄/H₂O ternary systems based on mutual solubility, and this model performs well for CO₂/H₂O binary mixtures. However, our experience in applying Chen and Yang (2019)'s model shows that some breaking points can be observed in the predicted IFT curves under some conditions, hampering its ability in providing consistent and smooth IFT predictions. In addition, using two sets of BIPs (as applied in Chen and Yang (2019)'s study) in the aqueous phase and non-aqueous phase can lead to thermodynamic inconsistency issue near the critical region as demonstrated by Li and Li (2019).

The discussion above reveals that the previous studies of phase behavior modeling of the $\rm CO_2/H_2O$ mixtures tend to primarily focus on phase-composition modeling and pay less attention to phase-density calculations (especially for the $\rm CO_2$ -rich phase). Whereas, phase-density is one important property in VLE and LLE since IFT calculations and flow simulations can heavily rely on such property. As for the IFT modeling, we are currently lacking a reliable IFT correlation that not only pays due tribute to the phase composition and density of $\rm CO_2/H_2O$ mixtures but also gives smooth and



consistent IFT predictions over a wider range of temperature/pressure conditions.

In this study, we first conduct a thorough literature review to select the most promising thermodynamic models that can well capture the VLE and LLE of $\mathrm{CO_2/H_2O}$ mixtures. Then, we conduct phase-composition calculations by using PR EOS, Twu α function, and Huron-Vidal mixing rule [as suggested by Aasen et al. (2017)], and validate the accuracy of this model by comparing the calculated VLE and LLE phase compositions to the measured ones. Then, we introduce Abudour et al. (2012b, 2013) volume translation model in phase-density calculations to check if applying this model can further improve the density-prediction accuracies. A new empirical IFT correlation for $\mathrm{CO_2/H_2O}$ mixtures is then proposed based on the reliable thermodynamic model that incorporates the Huron-Vidal mixing rule and the Abudour et al. (2013) volume translation model.

2 Methodology

2.1 PR EOS and α functions

In this study, PR EOS (Peng and Robinson 1976) is implemented because of its simplicity and more accurate liquid-density predictions compared with SRK EOS (Aasen et al. 2017). The expression of PR EOS is detailed in "Appendix A".

With regards to α functions in PR EOS, Twu α function and Gasem α function are used in this study. Compared with the other types of α functions, the Twu α function can describe the thermodynamic properties of polar compounds more accurately and perform better in the supercritical region (Young et al. 2016). In addition, according to the study by Aasen et al. (2017), Twu α function coupled with PR EOS and Huron-Vidal mixing rule yields the most accurate phase-composition estimations on CO_2/H_2O mixtures among the models evaluated by them. Therefore, we select Twu α function as one of the evaluated α functions in this study.

The Gasem α function provides more accurate representation of supercritical phase behavior (Gasem et al. 2001). Besides, based on the study by Abudour et al. (2013), Gasem α function coupled with PR EOS, vdW mixing rule and Abudour volume translation yields the most accurate liquid-phase-density predictions for the chemical compounds examined by their study. Therefore, we select the Twu α function and the Gasem α function in VLE/LLE and phase-density calculations. "Appendix A" shows the expressions of Twu α function and Gasem α function.

2.2 Mixing rules

Mixing rules have a great impact on phase equilibrium calculations. Huron and Vidal (1979) proposed a new expression by considering the excess Gibbs energy for CEOS, which made more accurate the phase-composition predictions for mixtures containing polar substances. Furthermore, according to the comprehensive study by Aasen et al. (2017), the most accurate thermodynamic model among the ones examined by them is PR EOS coupled with Twu α function and Huron-Vidal mixing rule, which provides an AAD of 4.5% in reproducing the phase-composition data measured for CO₂/H₂O mixtures. Hence, in the first part of this study, we collect more phase equilibria data for CO₂/H₂O mixtures to verify the performance of the model suggested by Aasen et al. (2017). These additional experimental data are not included in the study by Aasen et al. (2017).

The vdW mixing rule is one of the most commonly used mixing rules in petroleum industry (Pedersen et al. 2014). Although vdW mixing rule is originally developed for nonpolar systems, the vdW mixing rule coupled with the tuned BIPs can be reliably used for describing the phase behavior of mixtures containing polar components (e.g., water). Besides, based on the study by Abudour et al. (2012a), Gasem α function with vdW mixing rule and their temperature-dependent volume translation function provided a promising means to well reproduce the measured liquidphase densities for CO₂/H₂O mixtures. Therefore, in this study, we also employ the model suggested by Abudour et al. (2012a) to test if it outperforms the model suggested by Aasen et al. (2017). The expressions of vdW mixing rule and Huron-Vidal mixing rule and their BIPs are detailed in "Appendices B and C".

2.3 Volume translation models

Volume translation is used to overcome the inherent deficiency of CEOS in liquid-phase-density predictions. In order to improve liquid-phase-density calculations, Peneloux et al. (1982) developed a constant volume translation model in SRK EOS, while Jhaveri and Youngren (1988) developed a constant volume translation model in PR EOS. Abudour et al. (2012b, 2013) revised the temperature-dependent volume translation function to improve both saturated and single-phase liquid density calculations. Furthermore, unlike other temperature-dependent volume translation models, the volume translation model developed by Abudour et al. (2012b, 2013) does not yield thermodynamic inconsistency issues unless at extremely high pressures. Therefore, we select the constant and Abudour et al. volume translation models in this study for phase-density predictions. The expressions of these two volume translation models are detailed in "Appendix D".



2.4 IFT correlations for CO₂/H₂O mixtures

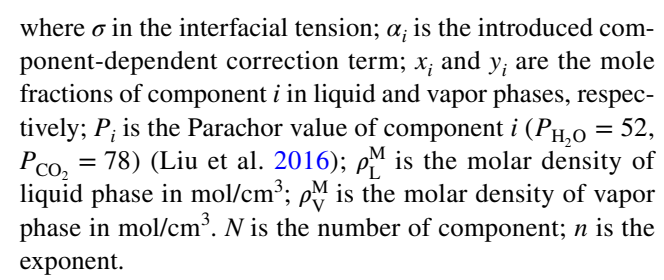
In this study, we select Parachor model (Sugden 1930), Hebach et al. (2002)'s correlation, and Chen and Yang (2019)'s correlation to predict IFT of CO₂/H₂O mixtures. The Parachor model (Sugden 1930) is one of the most widely used methods in determining mixtures' IFT. It correlates IFT with phase compositions and molar densities of each phase. Parachor is a component-dependent constant. The expression of the Parachor model is shown in "Appendix E". Hebach et al. (2002)'s correlation correlates IFT with temperature, pressure, and phase densities. Phase compositions are not included in their correlation. To make fair comparison, we also refit coefficients in their correlation based on the IFT database employed in this study. Values of the original and refitted coefficients as well as the Hebach et al. (2002)'s correlation are shown in "Appendix E".

Chen and Yang (2019)'s correlation correlates IFT with phase equilibrium ratios (K-values) and the reduced pressure of CO₂. Unlike the Parachor model and the Hebach et al. (2002)'s correlation, the density of the two equilibrating phases is not one input in the Chen and Yang (2019)'s correlation. Chen and Yang (2019)'s correlation, they proposed four groups of coefficient sets, i.e., one coefficient set (using one coefficient set on the whole pressure range) with or without the reduced pressure term, and two coefficient sets (dedicated to the pressure ranges of $p \le 73.8$ and p > 73.8 bar) with or without the reduced pressure term. Since using the reduced pressure term can improve prediction accuracy (Chen and Yang 2019), we introduce the reduced pressure term in this study. Similarly, we refit these coefficients based on the IFT databased employed in this study to make fair comparison. Values of the original and refitted coefficients as well as the Chen and Yang (2019)'s correlation are detailed in "Appendix E".

2.5 IFT correlation proposed in this study

Before we finalize our IFT correlation, we tried several scenarios to find the optimal one to correlate the IFT of CO_2/H_2O mixtures. Since the Parachor model is one of the most widely used models in mixtures' IFT predictions, we revise the original Parachor model by introducing a component-dependent correction term α_i ; furthermore, we replace the constant exponential term in the original Parachor model by correlating it with several physical properties (e.g., equilibrium ratios). The new IFT correlation can be expressed as follows:

$$\sigma = \left[\sum_{i=1}^{N} \alpha_i P_i (x_i \rho_{\mathcal{L}}^{\mathcal{M}} - y_i \rho_{\mathcal{V}}^{\mathcal{M}}) \right]^n$$
 (1)



First, the component-dependent correction term α_i is set as a constant for each component, and the exponential term n can be expressed by the equilibrium ratios of CO_2 -rich phase and aqueous phase:

$$n = C_1 \ln K_{\text{CO}_2} + C_2 \ln K_{\text{H}_2\text{O}} + C_3 \tag{2}$$

where C_1 , C_2 , and C_3 are empirical coefficients; K_{CO_2} and K_{H_2O} are the equilibrium ratios (as known as K-values) of CO_2 and H_2O :

$$K_i = y_i / x_i \tag{3}$$

Since using one coefficient set for both α_i and n on the whole CO₂-rich-phse density range cannot converge after reaching the maximum iterations, we use two coefficient sets based on CO₂-rich-phase densities. Table 1 listed the values of these coefficients and α_i determined by fitting the proposed correlation (abbreviated as Scenario #1) to the IFT training dataset.

Since using constants to represent α_i leads to a larger AAD compared with the refitted Chen and Yang (2019)'s correlation (i.e., 8.8746% vs. 7.8520%, respectively), we correlate equilibrium ratios to α_i to see if it can improve the IFT predictions. The expression of n in this scenario (abbreviated as Scenario #2) is the same as that in Scenario #1. The expression for α_i is given as:

$$\alpha_i = C_1 \ln K_{\text{CO}_2} + C_2 \ln K_{\text{H}_2\text{O}} + C_3 \tag{4}$$

Specifically, when the CO_2 -rich-phase density is greater than 0.2 g/cm³, α_{H_2O} can be simplified as:

$$\alpha_{\rm H_{2O}} = C_1 \ln K_{\rm CO_2} + C_3 \tag{5}$$

Table 1 Values of the correlation coefficients and α_i in Scenario #1

Coefficients	$\rho_{\rm CO_2\text{-rich}} < 0.2 \text{ g/cm}^{3a}$	$\rho_{\rm H_2O\text{-rich}} \ge 0.2 \text{ g/cm}^3$
$\alpha_{ m CO_2}$	0.7957	0.1520
$\alpha_{ m H_2O}$	0.8855	0.9509
C_1	-0.0727	0.1026
C_2	0.1044	0.0736
C_3	5.5730	3.9154

 $^{^{}a}\rho_{\text{CO}_2\text{-rich}}$ is the density of CO₂-rich phase



Table 2 listed the values of these coefficients determined by fitting the proposed correlation to the IFT training dataset. Since using one coefficient set for α_i and n on the whole CO_2 -rich-phse density range in Scenario #2 cannot converge after reaching the maximum iterations, we use two coefficients based on CO_2 -rich-phase densities (the same as Scenario #1).

We find that using correlations to represent α_i can slightly improve the IFT predictions (i.e., AAD of 8.31% in Scenario #2 vs. AAD of 8.87% in Scenario #1). Besides, we find that the value of n is around 4 over a wide range of temperature/pressure conditions in all scenarios (i.e., its value only slightly changes with the change of equilibrium ratios); therefore, we set the value of n as 4 for simplicity.

However, our experience in applying Scenarios #1 and #2 shows that some breaking points can be observed in the correlated IFT curves due to the fact that two different sets of coefficients are adopted under the conditions of $\rho_{\text{CO}_2\text{-rich}} < 0.2 \text{ g/cm}^3$ and $\rho_{\text{H}_2\text{O}\text{-rich}} \ge 0.2 \text{ g/cm}^3$, respectively. In addition, based on the study by Chen and Yang (2019), introducing the reduced pressure of CO_2 can improve IFT predictions. Thus, we introduce the reduced pressure of CO_2 in the expressions of α_i and use one coefficient set to see if these settings can further improve the prediction accuracies without yielding inconsistent IFT predictions. Based on the calculation results, the following IFT correlation yields the lowest AAD among the ones examined in this study:

$$\sigma = \left[\sum_{i=1}^{N} \alpha_i P_i \left(x_i \rho_{\mathcal{L}}^{\mathcal{M}} - y_i \rho_{\mathcal{V}}^{\mathcal{M}} \right) \right]^4 \tag{6}$$

where the α_i term in the new correlation can be expressed as:

$$\alpha = C_1 + (C_2 p_r + C_3) \ln K_{\text{CO}_2} + (C_4 p_r + C_5) \ln K_{\text{H}_2\text{O}}$$
 (7)

where p_r is the reduced pressure of CO₂.

Table 3 lists the values of these coefficients determined by fitting the proposed correlation to the IFT training dataset.

Table 3 Coefficients in the α_i term for H₂O and CO₂

Component	C_1	C_2	C_3	C_4	C_5
H ₂ O	1.1325	-0.0085	-0.0083	0.0134	0.0089
CO_2	-0.4193	-0.0057	-0.0320	0.0209	-0.1430

3 Results and discussion

The values of critical pressure (p_c) , critical temperature (T_c) , acentric factor (ω) , molecular weight (M), critical compressibility factor (Z_c) used in this study are retrieved from the NIST database (Lemmon et al. 2011).

3.1 Performance comparison of thermodynamic models in phase equilibrium calculations

Table 4 summarizes the measured phase equilibrium data of CO_2/H_2O mixtures over 278–378.15 K and 0.92–709.3 bar reported in the literature. Note that these experimental data were not included in the study by Aasen et al. (2017). Comparison between the measured and calculated phase-composition results is evaluated by the average absolute percentage deviation (AAD) defined as:

$$AAD = \frac{1}{N} \sum_{i}^{N} \left| \frac{x_{CAL} - x_{EXP}}{x_{EXP}} \right|_{i} \times 100\%$$
 (8)

where AAD is the average absolute percentage deviation; N is the number of data points; x_{CAL} and x_{EXP} are the calculated and measured mole fraction of CO_2 or H_2O in the aqueous phase (or the CO_2 -rich phase), respectively.

Table 5 details the settings of the four thermodynamic models examined in this work. Table 6 summarizes the performance of different thermodynamic models in phase-composition predictions.

As shown in Table 6, although AAD for $x_{\rm CO_2}$ of Case 3 (Twu + HV) is slightly higher than that of Case 4 (Gasem + HV), i.e., 4.73% of Case 3 vs. 3.64% of Case 4, Case 3 (Twu + HV) significantly outperforms the other models in $y_{\rm H_2O}$ predictions, i.e., AAD of 10.37% of Case 3 vs. > 16% of other cases. Thus, given the overall performance, Case 3 (Twu + HV) is found to be the best model

Table 2 Values of the correlation coefficients and α_i in Scenario #2

Coefficients	$ \rho_{\rm CO_2\text{-rich}} < 0.2 $	$ \rho_{\rm CO_2\text{-rich}} < 0.2 \text{ g/cm}^3 $			$\rho_{\rm H_2O\text{-rich}} \ge 0.2 \text{ g/cm}^3$		
	$\overline{C_1}$	C_2	C_3	$\overline{C_1}$	C_2	C_3	
a_{CO_2}	-0.4685	-0.2177	1.7944	0.4583	0.0107	-1.3451	
$\alpha_{ m H_2O}$	-0.1033	0.0311	1.8397	0.5259	_	-0.3583	
n	0.3599	-0.0855	1.3153	-0.2685	0.0124	3.5123	



Table 4 Phase equilibrium data of CO₂/H₂O mixtures employed in this study

T, K	p, bar	x_{CO_2} , $\%^{\text{a}}$	$y_{\rm H_2O}$, % ^b	N	References	AAD, % ^c
323.15–373.15	25.3–709.3	0.429-3.002	_	29 ^d	Weibe and Gaddy (1939)	2.09
285.15-313.15	25.3-506.6	0.925-3.196	_	42 ^e	Weibe and Gaddy (1940)	5.50
323.15-373.15	200-500	2-2.8	1–3	4^{f}	Tödheide and Frank (1962)	1.90/34.69
288.71-366.45	6.9-202.7	0.0973-2.63	0.0819-12.03	24 ^g	Gillepsie and Wilson (1982)	6.68/5.93
323.15	68.2-176.8	1.651-2.262	0.339-0.643	8	Briones et al. (1987)	3.17/5.26
285.15-304.21	6.9-103.4	_	0.0603-0.33739	9^{h}	Song and Kobayashi (1987)	6.40
323.15-378.15	101.33-152	1.56-2.1	0.55-0.9	4	D'Souza et al. (1988)	4.62/16.81
348.15	103.4-209.4	1.91-1.92	0.63-0.84	2/3 ⁱ	Sako et al. (1991)	7.97/25.38
323.15	101-301	2.075-2.514	0.547-0.782	3	Dohrn et al. (1993)	1.85/15.53
278-293	64.4-294.9	2.5-3.49	_	24	Teng et al. (1997)	7.36
288-323	0.92-4.73	0.038-0.365	_	49	Dalmolin et al. (2006)	2.89
313.2-343.2	43.3-183.4	1.13-2.40	_	28	Han et al. (2009)	3.37
273.15-573.15	100-1200	0.89-14.96	_	130	Guo et al. (2014)	5.43
323.15-423.15	150	1.77-2.19	_	3^{j}	Zhao et al. (2015)	4.18

^aSolubility of CO₂ in the aqueous phase

Table 5 Settings of four thermodynamic models examined in this work

Case No.	α function	Mixing rule	BIPs
Case 1	Gasem et al. (2001)	vdW (1873)	$kc_{ij} = 0.27$; $kd_{ij} = -0.21$ (Abudour et al. 2012a)
Case 2	Gasem et al. (2001)	vdW (1873)	$kc_{ij}(T)$; $kd_{ij}(T)^{a}$ (Abudour et al. 2012a)
Case 3	Twu et al. (1991)	Huron and Vidal (1979)	Aasen et al. (2017)
Case 4	Gasem et al. (2001)	Huron and Vidal (1979)	Aasen et al. (2017)

^aThe expressions of $kc_{ii}(T)$ and $kd_{ii}(T)$ are listed in "Appendix B"

in phase-composition predictions. Figure 1 compares the performance of different models at T = 323.15 K and T = 348.15 K. As can be seen from these two figures, the thermodynamic model Case 3 (Twu + HV) can well capture the trend exhibited by the measured solubility data over a wide pressure range.

Table 6 AAD of calculated mole fraction of CO_2 in the aqueous phase (x_{CO_2}) and mole fraction of H_2O in the CO_2 -rich phase (y_{H_2O}) by different thermodynamic models

Case No.	AAD for x_{CO_2} , %	AAD for $y_{\rm H_2O}$, %
Case 1	57.81	19.26
Case 2	8.85	16.90
Case 3	4.73	10.37
Case 4	3.64	16.59

3.2 Evaluation of thermodynamic models in density calculations

Table 7 summarizes the experimental aqueous-phase and CO_2 -rich-phase densities of $\mathrm{CO}_2/\mathrm{H}_2\mathrm{O}$ mixtures over 278–478.35 K and 2.5–1291.1 bar documented in the literature. The pressure–temperature coverage of the phase density data collected from the literature are shown in "Appendix F".

Since Case 3 (Twu+HV) outperforms other thermodynamic models in phase-composition predictions for CO_2/H_2O mixtures, we only focus on the performance of Case 3 coupled with volume translation in phase-density predictions. Table 8 summarizes the performance of different volume translation models in both aqueous-phase and CO_2 -rich-phase density calculations.



^bSolubility of H₂O in CO₂-rich phase

^cAAD yielded by the Case 3 model (PR EOS, Twu α function, and Huron–Vidal mixing rule) in x_{CO_2} and/or $y_{\text{H}_2\text{O}}$ predictions. If two numbers are shown in table, the former indicates AAD in x_{CO_2} prediction and the latter indicates AAD in $y_{\text{H}_2\text{O}}$ prediction.

d,e,f,g,h,iThese data are already summarized by Spycher et al. (2003). We directly use these data mentioned in their paper for convenience

 $^{{}^{}i}N$ is 2 for x_{CO_2} and 3 for $y_{\text{H}_2\text{O}}$, respectively

^jOnly experimental data for CO₂/pure water are selected in the study by Zhao et al. (2015)

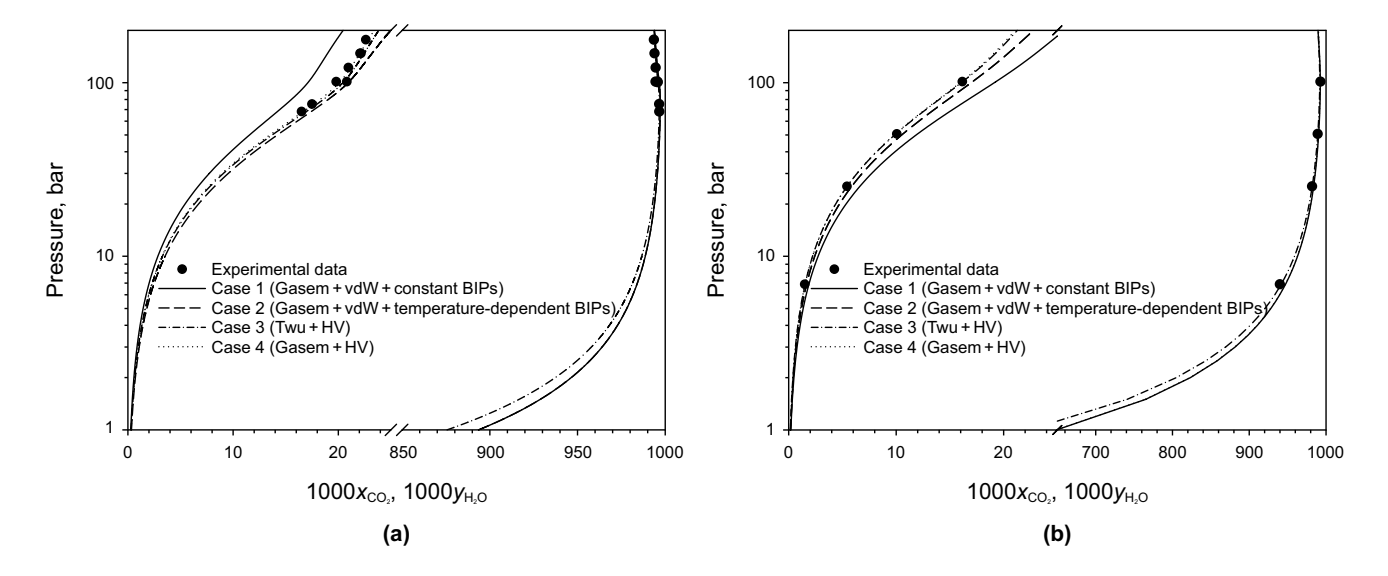


Fig. 1 Measured and calculated pressure-composition data for CO_2/H_2O mixtures at T=323.15 K (a) and T=348.15 K (b). Solid circles are the experimental data from the studies by Briones et al. (1987) and Gillepsie and Wilson (1982)

 $\textbf{Table 7} \quad \text{Aqueous-phase } (\rho_{H,O}) \text{ and } CO_2\text{-rich-phase } (\rho_{CO,\text{-rich}}) \text{ density data of } CO_2/H_2O \text{ mixtures employed in this study}$

T, K	p, bar	$\rho_{\rm H_2O}$, kg/m ³	$\rho_{\rm CO_2\text{-rich}}$, kg/m ³	N	References	AAD, % ^a
352.85–471.25	21.1–102.1	840–963	_	32	Nighswander et al. (1989)	3.01
288.15-298.15	60.8-202.7	1015-1027	_	27	King et al. (1992)	2.17
278-293	64.4-294.9	1013.68-1025.33	_	24	Teng et al. (1997)	1.35
304.1	10-70	999.4-1011.8	18.8-254.2	8	Yaginuma et al. (2000)	2.67/5.12
332.15	33.4-285.9	990.5-1010.3	_	29	Li et al. (2004)	3.80
283.8-333.19	10.8-306.6	983.7-1031.77	_	203	Hebach et al. (2004)	2.47
307.4-384.2	50-450	950.6-1026.1	80.8-987.5	43	Chiquet et al. (2007)	3.61/2.01
322.8-322.9	11-224.5	988.52-1009.13	18.8484-812.725	11	Kvamme et al. (2007)	3.37/1.94
382.41-478.35	34.82-1291.9	871.535-994.984	36.943-944.965	32/40 ^b	Tabasinejad et al. (2010)	4.85/4.43
298.15-333.15	14.8-207.9	984.6-1022	24.6-907.1	36	Bikkina et al. (2011)	3.08/3.15
292.7-449.6	2.5-638.9	905.9-1034.9	4.6-1023.4	145/128 ^c	Efika et al. (2016)	3.56/2.01

^aAAD yielded by Case 3–1 model (PR EOS, Twu α function, Huron–Vidal mixing rule, and Abudour volume translation model) for $\rho_{\text{H}_2\text{O}}$ and/or $\rho_{\text{CO}_2\text{-rich}}$ predictions. If two numbers are shown in table, the former indicates AAD for $\rho_{\text{H}_2\text{O}}$ prediction and the latter indicates AAD for $\rho_{\text{CO}_2\text{-rich}}$ prediction

As shown in Table 8, incorporation of VT into the thermodynamic framework can generally improve the phase-density prediction accuracy. Case 3–1 (Twu+HV+Abudour VT) provides the most accurate estimates of both aqueous-phase and CO₂-rich-phase density, yielding AAD of 2.90% in reproducing the measured phase-density data. Figure 2 further visualizes some of the calculation results by these three different models at different pressure/temperature conditions.

It can be seen from Fig. 2 that, regarding aqueousphase density predictions, the performance of Case 3–2 (Twu+HV+Constant VT) improves dramatically as temperature rises. As shown in Fig. 2e, f, at high temperature conditions, Cases 3–2 yields the most accurate aqueousphase density predictions; however, it fails to accurately predict CO₂-rich-phase densities. As a lighter phase, CO₂-rich-phase density can be accurately predicted without the use of volume translation functions. Applying Abudour VT method is able to only slightly improve the prediction



 $^{{}^{\}rm b}N$ is 30 for $\rho_{{
m H}_2{
m O}}$ and N is 40 for $\rho_{{
m CO}_2\text{-rich}}$

 $^{^{\}rm c}N$ is 144 for $ho_{
m H_2O}$ and N is 128 for $ho_{
m CO_2\text{-rich}}$

 $\textbf{Table 8} \quad \text{AAD of the calculated aqueous-phase density } (\rho_{\text{H},\text{O}}) \text{ and } \text{CO}_2\text{-rich-phase density } (\rho_{\text{CO}_2\text{-rich}}) \text{ by different thermodynamic models}$

Model	AAD for $\rho_{\mathrm{H_2O}}$, %	AAD for $ ho_{\mathrm{CO_2 ext{-}rich}}$,%	Average AAD, %
Case 3–1 (Twu+HV+Abudour VT ^a)	3.04	2.62	2.90
Case 3–2 (Twu+HV+Constant VT)	4.49	7.86	5.51
Case 3 (Base case) (Twu+HV)	15.08	3.38	11.44

^aVT: volume translation

accuracy (i.e., AAD of 2.62%). In contrast, applying constant VT in CO_2 -rich-phase density predictions can lead to larger errors than the case without the use of VT.

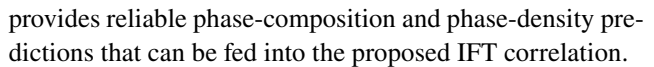
Figure 3 compares the performance of different models in terms of their accuracy in phase-density predictions over 382.14–478.35 K and 35.3–1291.9 bar. Note that the results of CPA EOS model from the work by Tabasinejad et al. (2010) focuses on the same pressure and temperature ranges. As can be seen from Fig. 3, although the CPA EOS model can accurately predict the aqueous-phase density, it tends to be less accurate in determining the CO₂-rich-phase density. Overall, the thermodynamic model Cases 3–1 (Twu+HV+Abudour VT) give an accuracy comparable to the more complex CPA EOS model.

In addition, according to the study by Aasen et al. (2017), CPA EOS model yields higher percentage errors (AAD) in reproducing phase-composition data for $\mathrm{CO_2/H_2O}$ mixtures compared with Case 3 (PR EOS + Twu + HV), i.e., 9.5% vs. 4.5% (Aasen et al. 2017). Therefore, overall, Case 3–1 (Twu + HV + Abudour VT) is a more accurate model in both phase-composition and phase-density predictions for $\mathrm{CO_2/H_2O}$ mixtures.

3.3 Evaluation of the newly proposed IFT correlation

Table 9 summarizes the experimental IFT data of $\rm CO_2/H_2O$ mixtures over 278.15–477.59 K and 1–1200.96 bar documented in the literature. Ideally, phase densities should be directly measured; however, only Chiquet et al. (2007), Kvamme et al. (2007), Bikkina et al. (2011), Bachu and Bennion (2009), and Shariat et al. (2012) applied measured phase densities in IFT calculations. In order to expand our IFT database, IFT data with precisely determined phase densities are also included in our IFT database. The collected IFT data are randomly placed into two bins: a training dataset (including 589 data points) and a validation dataset (including 189 data points).

Results in Sects. 3.1 and 3.2 reveal that the thermodynamic model using PR EOS, Twu α function, Huron-Vidal mixing rule, and Abudour et al. (2013) VT yields the most accurate estimates on both phase compositions and densities. Therefore, the aforementioned thermodynamic model



Mean absolute errors (MAE), AAD, and coefficient of determination (R^2) are used as performance measures. The expressions of MAE and R^2 are as follows:

$$MAE = \frac{1}{N} \sum_{i=1}^{N} |\sigma_{EXP,i} - \sigma_{CAL,i}|$$
(9)

$$R^{2} = 1 - \frac{\sum_{i=1}^{N} \left(\sigma_{\text{EXP},i} - \sigma_{\text{CAL},i}\right)^{2}}{\sum_{i=1}^{N} \left(\sigma_{\text{EXP},i} - \overline{\sigma}_{\text{EXP}}\right)^{2}}$$
(10)

where $\sigma_{\rm EXP}$ is the measured IFT data in mN/m; $\sigma_{\rm CAL}$ is the calculated IFT in mN/m by different correlations; $\overline{\sigma}_{\rm EXP}$ is the average of the measured IFTs in mN/m.

3.3.1 Performance of different IFT correlations

Table 10 shows the details of the different IFT models examined in this study. Table 11 summarize the performance of different correlations in IFT estimations. As can be seen, the most accurate IFT model is Model 3 proposed in this study, although it only shows a marginal edge over Model 2.

Figure 4 visually compares the measured IFTs vs. pressure and the calculated ones by different IFT models at selected temperatures. As shown in these plots, in general, Model 3 (this study) outperforms other empirical correlations over a wide range of temperatures and pressures. It can be also observed from these plots that breaking points appear in the predicted IFT curves at p = 73.8 bar by Model 2 (Refitted Chen and Yang (2019)'s correlation with two coefficient sets). Such discontinuous IFT prediction can be attributed to the fact that two different sets of coefficients are adopted under the conditions of $p \le 73.8$ and p > 73.8 bar, respectively, in Chen and Yang (2019)'s correlation. Although using one coefficient in Chen and Yang (2019)'s correlation (e.g., Model 5) can avoid such discontinuous IFT predictions, it yields larger percentage errors. Therefore, Model 3 (this study) is the best model in IFT predictions for CO_2/H_2O mixtures over a wide range of temperatures and pressures.

Figure 5 illustrates how the IFTs predicted by Model 3 (this study) vary with pressure at different temperatures. It can be observed from Fig. 5 that the new IFT correlation



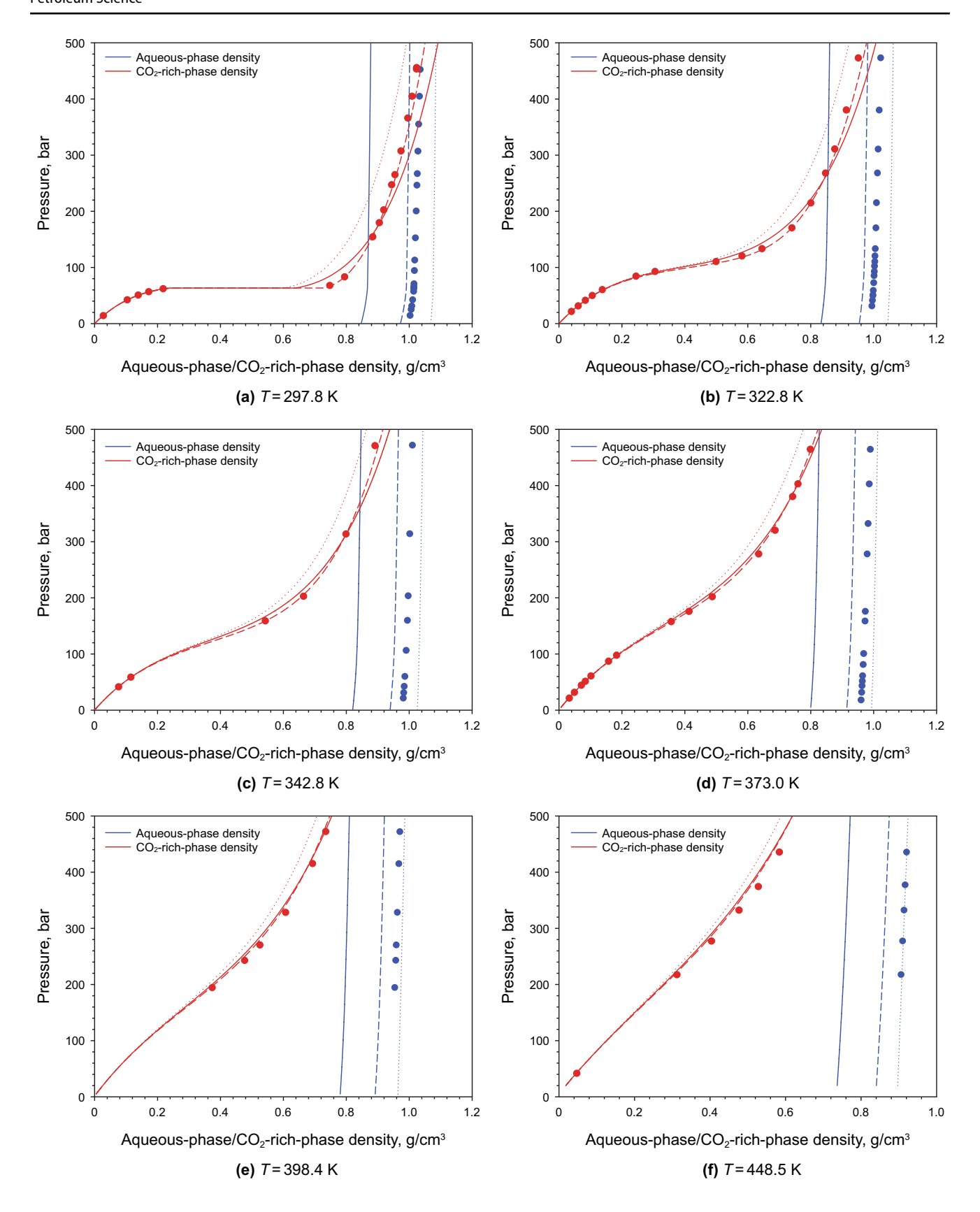


Fig. 2 Predictions of aqueous-phase and CO_2 -rich-phase density by Case 3–1 (Twu+HV+Abudour VT, dashed line), Case 3–2 (Twu+HV+constant VT, dotted line) and Case 3 (Base case, solid line) at different temperature conditions. The circles are the measured phase-density data from the study by Efika et al. (2016)



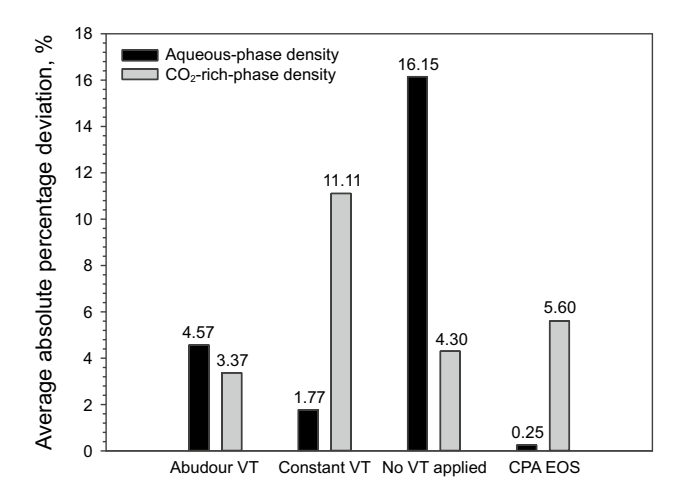


Fig. 3 Bar chart plots comparing the AAD in aqueous-phase (black) and $\rm CO_2$ -rich-phase (gray) density predictions by different models over 382.14–478.35 K and 35.3–1291.9 bar. Calculation results by the CPA EOS method are from the study by Tabasinejad et al. (2010)

provides smooth and consistent IFT predictions at different pressures and temperatures. Overall, Model 3 proposed in this study yields accurate and consistent IFT predictions over the wide range of temperatures and pressures, although it yields relatively higher percentage errors at higher temperature conditions (e.g., T = 478 K) compared with that at

lower temperature conditions (i.e., T < 378 K). It is interesting to observe from Fig. 5a that when the pressure is less than around 15 bar and the temperature is between 278.15 and 368.15 K, an increase in temperature leads to a decrease in the predicted IFT under the same pressure. In comparison, when the pressure is larger than around 15 bar, an increase in temperature leads to an increase in the predicted IFT. At higher temperatures of 378.15-478.15 K, an increase in temperature always results in a decline in the predicted IFT under the same pressure, as seen in Fig. 5b. Most of the measured IFTs documented in the literature follow this trend (Akutsu et al. 2007; Chalbaud et al. 2009; Chiquet et al. 2007; Chun and Wilkinson 1995; Da Rocha et al. 1999; Georgiadis et al. 2010; Hebach et al. 2002; Heuer 1957; Hough et al. 1959; Kvamme et al. 2007; Khosharay and Varaminian 2014; Liu et al. 2016; Park et al. 2005; Pereira et al. 2016; Shariat et al. 2012), except for the studies by Bachu and Bennion (2009) and Bikkina et al. (2011), i.e., an increase in temperature leads to an increase in IFT at a temperature range of 373.15-398.15 K in the study by Bachu and Bennion (2009), and an increase in temperature leads to an increase in IFT over 298.15-333.15 K in the study by Bikkina et al. (2011). Again, the sharp drops in the IFT curves at lower temperatures (where CO₂ remains subcritical) are due to the transformation of VLE to LLE.

Table 9 Measured IFT data for CO₂/H₂O mixtures used in this study

T, K	p, bar	IFT, mN/m	N	References	AAD, % ^a
311–411	1–689.48	17.40–58.40	58 ^b	Heuer (1957)	9.13
311.15-344.15	1-197.8	17.63-69.20	28°	Hough et al. (1959)	16.73
278.15-344.15	1-186.1	18.27-74.27	114 ^d	Chun and Wilkinson (1995)	6.18
311.15-344.15	1.6-310.7	19.38-56.86	20 ^e	Da Rocha et al. (1999)	13.26
278.4-333.3	1-200.3	12.4–74	85	Hebach et al. (2002)	3.76
293.15-344.15	1-173.2	20.55-78.01	$26^{\rm f}$	Park et al. (2005)	7.19
318.15	11.6-165.6	25.4-70.5	14	Akutsu et al. (2007)	8.38
322.8-322.9	11–224.5	29.1-63.7	11	Kvamme et al. (2007)	4.80
307.4-384.2	50-450	45.8-22.8	43	Chiquet et al. (2007)	8.57
293.15-398.15	20-270	18.9-68.1	87 ^g	Bachu and Bennion (2009)	8.89
344.15	28.57-245.24	25.49-45.01	11	Chalbaud et al. (2009)	10.86
297.8-374.3	10-600.6	21.23-65.73	80	Georgiadis et al. (2010)	3.13
298.15-333.15	14.8-207.9	22.16-59.66	36	Bikkina et al. (2011)	11.29
323.15-477.59	77.78-1200.96	10.37-35.38	21	Shariat et al. (2012)	15.89
284.15-312.15	10-60	29.02-66.98	30	Khosharay and Varaminian (2014)	3.37
298.4-469.4	3.4-691.4	12.65-68.52	78	Pereira et al. (2016)	6.46
299.8-398.15	7.86–344.12	28.04-68.23	36	Liu et al. (2016)	9.89

^aAAD of the new IFT correlation proposed in this study (abbreviated as Model 3)

d.f.gSome experimental data appear to be outliers and hence excluded for further analysis due to the significant deviation from other experimental data at similar temperature and pressure conditions (see Appendix G)



b.c.e These data are already summarized by Park et al. (2005) and Shariat et al. (2012). We directly use these data mentioned in their papers for convenience

Table 10 Technical Characteristics of different IFT models examined in this study

IFT model No.	Characteristics
Model 1	Original Parachor model
Model 2	Refitted Chen and Yang (2019)'s correlation with two coefficient sets
Model 3	Newly proposed correlation (this study)
Model 4	Refitted Hebach et al. (2002)'s correlation
Model 5	Refitted Chen and Yang (2019)'s correlation with one coefficient set

3.3.2 Statistical significance tests of IFT correlations

As shown in Table 11, the AADs yielded by Model 2 (refitted Chen and Yang (2019)'s correlation) and Model 3 (this study) are on the same scale. Therefore, it is necessary to conduct statistical significance tests to check if the marginal edge of Model 3 over Model 2 is statistically significant. Figure 1 shows the frequency distribution of the differences between the measured IFT data (i.e., whole dataset including 778 data points) and calculated ones by Model 2, while Fig. 7 shows the same information for Model 3. As can be seen from Figs. 6 and 7, the distribution of the deviations generated by the two models can be considered to follow Gaussian distributions. As such, paired one-tailed t-tests are applied as the statistical significance test method (Japkowicz and Shah 2011).

P-value is used to check if one model is better than another one. Typically, the significance threshold α is 0.05; when $P > \alpha$, two models have the same performance. In contrast, when $P \le \alpha$, it is reasonable to say that one model is significantly better than another one (Japkowicz and Shah 2011).

P-value of Model 2 (refitted original Chen and Yang (2019)'s correlation with two coefficient sets) and Model 3

(this study) is 0.0069, $P < \alpha$ ($\alpha = 0.05$); therefore, it is reasonable to say that Model 3 statistically outperforms Model 2. In addition, the new model does not give discontinuous IFT predictions, while Chen and Yang (2019)'s IFT model bears such issue.

4 Conclusions

The objective of this study is to screen and develop reliable models for describing the VLE, LLE, phase density, and IFT of CO₂/H₂O mixtures. Based on the comparison between the experimental data and the calculated ones from different models, we can reach the following conclusions:

- The most accurate method to represent CO₂/H₂O VLE and LLE is PR EOS, Twu α function, and Huron-Vidal mixing rule, which only yields AAD of 5.49% and 2.90% in reproducing measured CO₂/H₂O phase-composition data and phase-density data over a temperature range of 278–378.15 and 278–478.35 K and over a pressure range of 6.9–709.3 and 2.5–1291.1 bar, respectively.
- Applying either constant or Abudour et al. (2013) VT method can significantly improve aqueous-phase density calculations. In addition, when the temperature is higher than 373 K, constant VT method can yield lower error in reproducing measured phase-density data than Abudour et al. (2013) VT method;
- Constant VT method cannot improve the prediction accuracy of CO₂-rich-phase density. Abudour et al. (2013) VT method can slightly improve CO₂-rich-phase density predictions, but such improvement is more obvious at low to moderate temperature conditions.
- 4. The new IFT correlation based on the aforementioned PR EOS model outperforms other empirical correlations with an overall AAD of 7.77% in reproducing measured IFT data of CO₂/H₂O mixtures. The new IFT correla-

Table 11 Summary of the performance of different correlations in IFT estimations

Evaluation metrics		Model 1 ^a	Model 2	Model 3	Model 4	Model 5
Training dataset	AAD, %	_	7.5218	6.6893	10.6901	11.4002
	MAE	-	2.4232	2.1311	3.2532	3.8349
	R^2	_	0.9416	0.9547	0.9008	0.8586
Validation dataset	AAD, %	_	8.8812	8.8684	11.6494	13.3408
	MAE	_	2.6446	2.6064	3.4174	4.1864
	R^2	_	0.9116	0.9325	0.9044	0.8402
Overall	AAD, %	47.0902	7.8520	7.7683	10.9231	11.8716
	MAE	13.7870	2.4770	2.3586	3.2931	3.9203
	R^2	-0.7053	0.9372	0.9420	0.9017	0.8541

^aNo refitted coefficients are applied in Parachor model. Instead, we directly apply Parachor model in IFT calculations. Thus, it is not necessary to distinguish between training and validation datasets



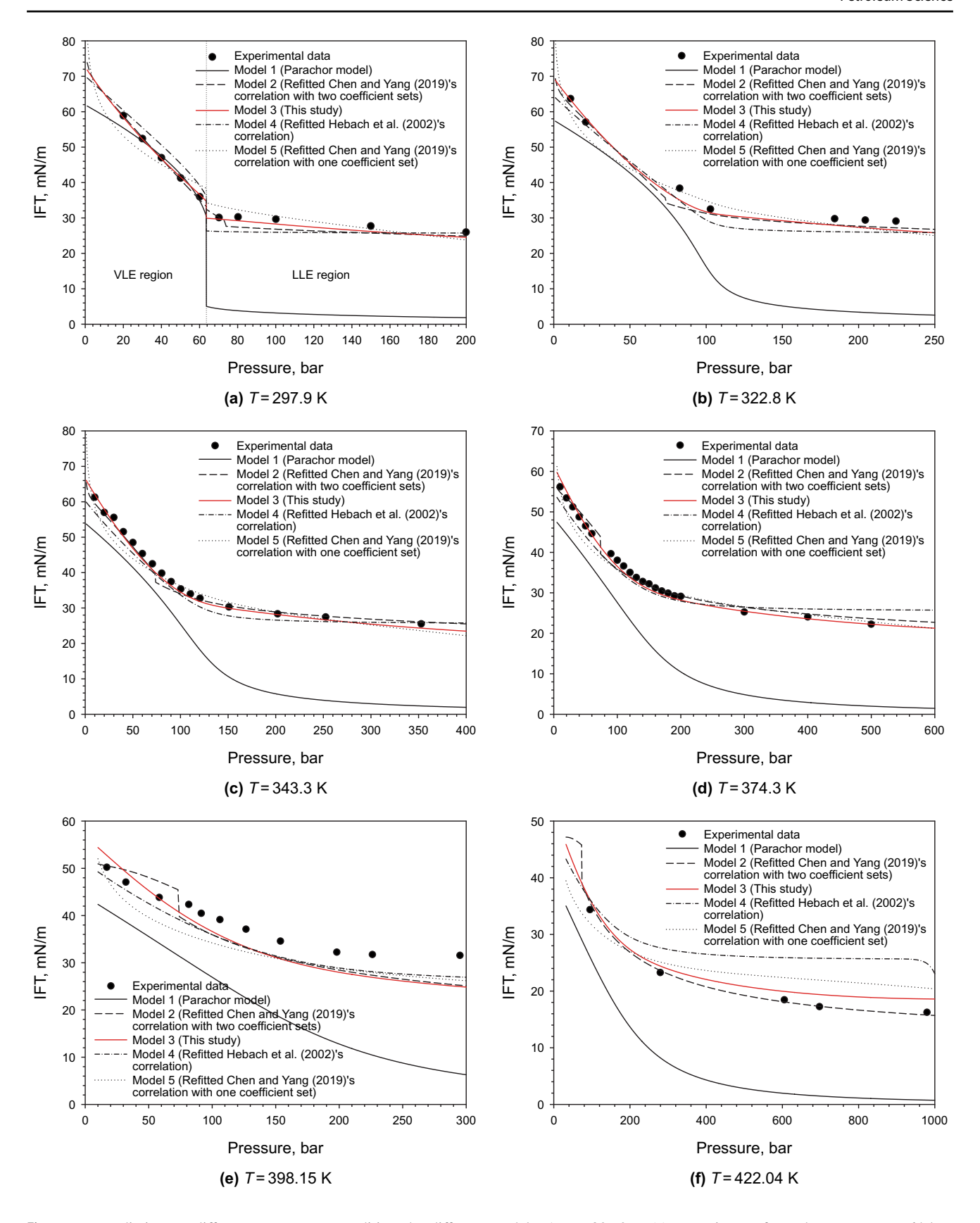


Fig. 4 IFT predictions at different temperature conditions by different models. At T=297.9 K (a), VLE is transformed to LLE at p=64 bar. Model 1 (Parachor model) shows a more deteriorating performance when the vapor CO_2 -rich phase changes to a liquid phase. Experimental data are from the studies by Kvamme et al. (2007), Georgiadis et al. (2010), Liu et al. (2016), and Shariat et al. (2012)



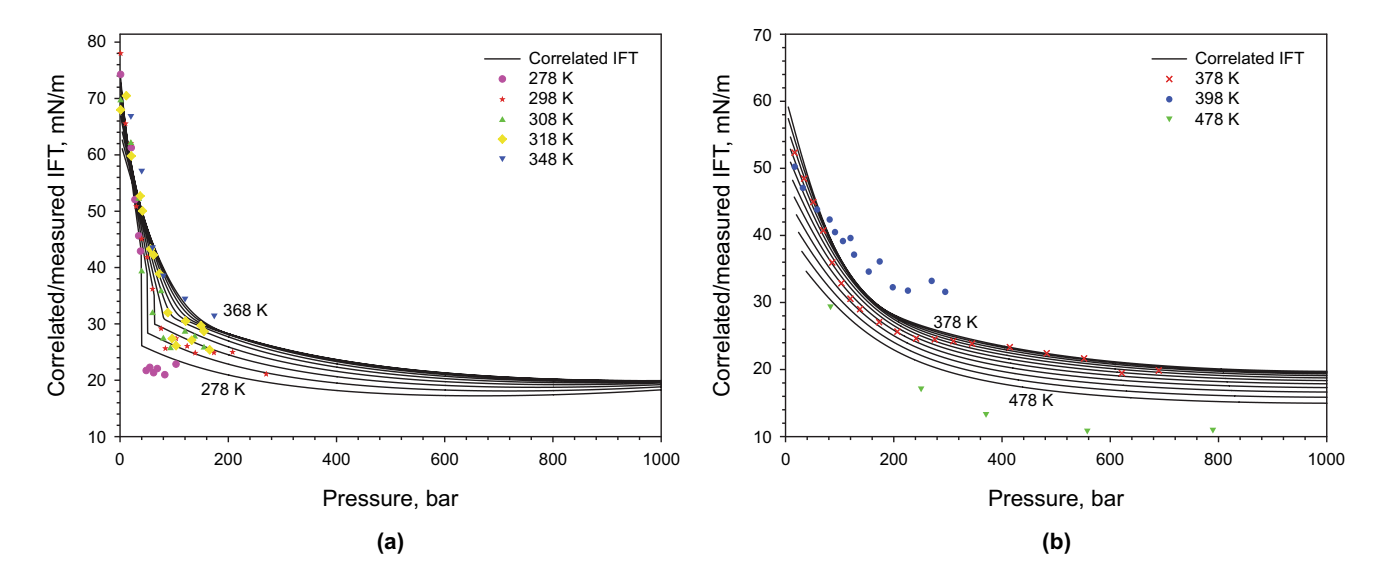


Fig. 5 Plots of predicted IFTs vs. pressure by the newly proposed IFT correlation Model 5 at the temperature ranges of 278–368 K (a) and 378–478 K (b). The curves are plotted with an interval of 10 K. Experimental data are taken from previous studies by Heuer (1957), Chun and Wilkinson (1995), Park et al. (2005), Akutsu et al. (2007), Bachu and Bennion (2009), Bikkina et al. (2011), Shariat et al. (2012), and Liu et al. (2016)

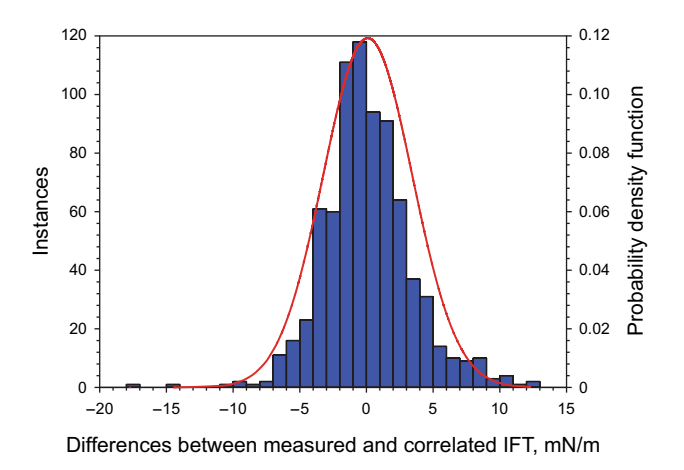


Fig. 6 Frequency distribution of the differences between the measured IFT data (i.e., the whole dataset including 778 data points) and calculated ones by Model 2 (refitted Chen and Yang (2019)'s correlation with two coefficient sets). Blue columns are instances, and the red curve is probability density function which follows Gaussian distribution with μ =0.0941 and σ^2 =3.3457

tion is only slightly more accurate than the refitted Chen and Yang (2019)'s correlation with two coefficient sets. But the new correlation yields smooth IFT predictions, avoiding the issue of discontinuous IFT predictions yielded by Chen and Yang (2019)'s correlation.

Open Access This article is licensed under a Creative Commons Attribution 4.0 International License, which permits use, sharing, adaptation, distribution and reproduction in any medium or format, as long

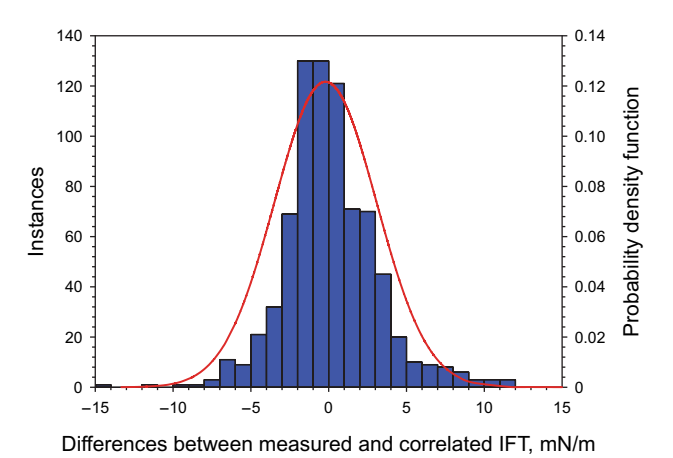


Fig. 7 Frequency distribution of the difference between the measured IFT data (i.e., the whole dataset including 778 data points) and calculated ones by Model 3 (this study). Blue columns are instances, and the red curve is probability density function which follows Gaussian distribution with μ =-0.2051 and σ ²=3.2781

as you give appropriate credit to the original author(s) and the source, provide a link to the Creative Commons licence, and indicate if changes were made. The images or other third party material in this article are included in the article's Creative Commons licence, unless indicated otherwise in a credit line to the material. If material is not included in the article's Creative Commons licence and your intended use is not permitted by statutory regulation or exceeds the permitted use, you will need to obtain permission directly from the copyright holder. To view a copy of this licence, visit http://creativecommons.org/licenses/by/4.0/.



Appendix A: PR EOS and α functions

The PR EOS (Peng and Robinson 1976) can be expressed as:

$$p = \frac{RT}{v - b} - \frac{a}{v(v + b) + b(v - b)}$$
 (11)

where p is the pressure in bar; v stands for the molar volume in cm³/mol; T is the temperature in K; a is the attraction parameter with unit of bar cm⁶/mol², and b is the repulsion parameter with unit of cm³/mol; a and b can be determined by Eqs. (12) and (13):

$$a = 0.457535 \frac{R^2 T_c^2}{p_c} \alpha \tag{12}$$

$$b = 0.077796 \frac{RT_{\rm c}}{p_{\rm c}} \tag{13}$$

where R is the universal gas constant in J/(mol K); $T_{\rm c}$ is the critical temperature in K; $p_{\rm c}$ is the critical pressure in bar; and α is the so-called alpha function.

The expression of Twu α function can be written as (Twu et al. 1991):

$$\alpha(T_{\rm r}) = T_{\rm r}^{N(M-1)} \exp\left[L\left(1 - T_{\rm r}^{MN}\right)\right] \tag{14}$$

where T_r is the reduced temperature; L, M and N are compound-specific parameters. The values of these parameters regressed by Martinez et al. (2018) are used in this study.

Gasem α function can be expressed by (Gasem et al. 2001):

$$\alpha(T) = \exp\left(\left(A + BT_{\rm r}\right)\left(1 - T_{\rm r}^{C + D\omega + E\omega^2}\right)\right) \tag{15}$$

where the values of correlation parameters A through E are 2.0, 0.836, 0.134, 0.508 and -0.0467, respectively.

Appendix B: Summary of van der Waals one-fluid mixing rule and its BIPs

The van der Waals one-fluid mixing rule can be expressed as (van der Waals 1873):

$$a_{\rm m} = \sum_{i=1}^{n} \sum_{j=1}^{n} z_i z_j \sqrt{a_i a_j} (1 - k c_{ij})$$
(16)

$$b_{\rm m} = \sum_{i=1}^{n} \sum_{j=1}^{n} z_i z_j \frac{\left(b_i + b_j\right)}{2} \left(1 + k d_{ij}\right) \tag{17}$$

where z_i is the molar fraction of the *i*th component in the mixture; a_i and b_i can be calculated by Eqs. (12) and (13);

Table 12 BIPs correlations in the van der Waals mixing rule as obtained by Abudour et al. (2012a, b)

Case No.	$kc_{ij} = AT + I$	3	$kd_{ij} = AT +$	В
	\overline{A}	В	\overline{A}	В
Case 2	0.00058	0.08149	0.00029	-0.31262

 kc_{ij} and kd_{ij} are the BIPs that need to be fitted. In this study, the linear temperature-dependent BIP correlations from the study by Abudour et al. (2012a, b) are applied for CO_2/H_2O mixtures. Table 12 lists the BIP correlations obtained by Abudour et al. (2012a, b).

When vdW mixing rule is used in PR EOS, the fugacity coefficient can be written as:

$$\ln \varphi_{i} = \frac{bb_{i}}{b_{m}}(Z - 1) - \ln(Z - B) - \frac{A}{2\sqrt{2}B} \left(\frac{2aa_{i}}{a_{m}} - \frac{bb_{i}}{b_{m}}\right) \ln \left(\frac{Z + \left(1 + \sqrt{2}\right)B}{Z - \left(1 + \sqrt{2}\right)B}\right)$$
(18)

where

$$bb_i = 2\sum_{i=1}^n z_j \frac{b_i + b_j}{2} (1 + kd_{ij}) - b_{m}$$
(19)

$$aa_i = \sum_{i=1}^n z_j \sqrt{a_i a_j} (1 - kc_{ij})$$
 (20)

where Z is the compressibility factor. For PR EOS, Z can be calculated by Eq. (21).

$$Z^{3} - (1 - B)Z^{2} + (A - 3B^{2} - 2B)Z - (AB - B^{2} - B^{3}) = 0$$
(21)

where

$$A = \frac{a_{\rm m}p}{R^2T^2} \tag{22}$$

$$B = \frac{b_{\rm m}p}{RT}. (23)$$

Appendix C: Summary of Huron-Vidal mixing rule and its BIPs

In the Huron-Vidal mixing rule, the following equations are applied to calculate a_m and b_m (Huron and Vidal 1979):

$$b_{\rm m} = \sum_{i=1}^{n} \sum_{j=1}^{n} z_i z_j \frac{(b_i + b_j)}{2}$$
 (24)



$$a_{\rm m} = b_{\rm m} \left[\sum_{i=1}^{n} z_i \frac{a_i}{b_i} - \frac{G_{\infty}^{\rm E}}{\Lambda} \right]$$
 (25)

where $G_{\infty}^{\rm E}$ is the excess Gibbs energy at infinite pressure, and Λ is an EOS-dependent parameter. For PR EOS, $\Lambda = 0.62323$ (Huron and Vidal 1979).

The excess Gibbs energy corresponding to the non-random two-liquid (NRTL) (Zhao and Lvov 2016; Wong and Sandler 1992) model can be expressed by (Aasen et al. 2017; Huron and Vidal 1979):

$$G_{\infty}^{E} = RT \sum_{i=1}^{n} z_{i} \frac{\sum_{j=1}^{n} \tau_{ji} b_{j} z_{j} \exp(-\alpha_{ji} \tau_{ji})}{\sum_{k=1}^{n} b_{k} z_{k} \exp(-\alpha_{ki} \tau_{ki})}$$
(26)

where

$$\tau_{ji} = \frac{\Delta g_{ji}}{RT} \tag{27}$$

$$g_{ii} = -\Lambda \frac{a_i}{b_i} \tag{28}$$

$$g_{ij} = -2\frac{\sqrt{b_i b_j}}{b_i + b_j} \sqrt{g_{ii} g_{jj}} (1 - k_{ij})$$
(29)

The generalized BIP correlations for τ_{ij} obtained by Aasen et al. (2017) are given below:

$$\frac{g_{12}}{RT_0} = 5.831 - 2.559 \left(\frac{T}{T_0}\right) \tag{30}$$

$$\frac{g_{21}}{RT_0} = -3.311 + 0.03770 \left(\frac{T}{T_0}\right) \tag{31}$$

where $T_0 = 1000 \text{ K}$ is the reference temperature.

When the Huron–Vidal mixing rule is used in PR EOS, the fugacity coefficient can be calculated by (Zhao and Lvov 2016):

The derivation of the expression of the activity coefficient in Huron-Vidal mixing rule is detailed in "Appendix H".

Appendix D: Summary of volume translation models applied in this study

The constant volume translation can be expressed as (Peneloux et al. 1982; Jhaveri and Youngren 1988):

$$v_{\text{corr}} = v_{\text{EOS}} - \sum_{i=1}^{n} z_i c_i$$
 (34)

where v_{corr} is corrected molar volume in cm³/mol; v_{EOS} stands for PR-EOS-calculated molar volume in cm³/mol; c_i is the component-dependent volume shift parameter which can be determined by Eq. (35) (Young et al. 2017).

$$c_i = s_i \times b_i \tag{35}$$

The values of s_i used by Liu et al. (2016) are applied in this study ($s_{H,O} = 0.23170$ and $s_{CO_2} = -0.15400$).

Abudour volume translation model can be expressed as (Abudour et al. 2012a, b):

$$v_{\text{corr}} = v_{\text{EOS}} + c - \delta_{\text{c}} \left(\frac{0.35}{0.35 + d} \right)$$
 (36)

where δ_c is volume correction at the critical temperature in cm³/mol; d is the dimensionless distance function given by (Mathias et al. 1989; Abudour et al. 2012b):

$$d = \frac{1}{RT_c} \left(\frac{\partial p^{\text{PR}}}{\partial \rho} \right)_T \tag{37}$$

where ρ is the molar density in mol/cm³. The volume translation function proposed by Abudour et al. (2013) was extended to mixtures by the following equations (Abudour et al. 2013):

$$\ln \varphi_i = \frac{b_i}{b_{\rm m}} (Z - 1) - \ln(Z - B) - \frac{1}{2\sqrt{2}} \left(\frac{a_i}{b_i RT} + \frac{\ln \gamma_i}{\Lambda} \right) \ln \left(\frac{Z + \left(1 + \sqrt{2} \right) B}{Z - \left(1 + \sqrt{2} \right) B} \right) \tag{32}$$

where $\ln \gamma_i$ is the activity coefficient of component *i* and can be expressed as (Zhao and Lvov 2016):

$$\ln \gamma_{i} = \frac{\sum_{j=1}^{n} \tau_{ji} z_{j} b_{j} \exp(-\alpha_{ji} \tau_{ji})}{\sum_{k=1}^{n} z_{k} b_{k} \exp(-\alpha_{ki} \tau_{ki})} + \sum_{j=1}^{n} \left[\frac{b_{i} z_{j} \exp(-\alpha_{ij} \tau_{ij})}{\sum_{k=1}^{n} z_{k} b_{k} \exp(-\alpha_{kj} \tau_{kj})} \cdot \left(\tau_{ij} - \frac{\sum_{l=1}^{n} \tau_{lj} z_{l} b_{l} \exp(-\alpha_{lj} \tau_{lj})}{\sum_{k=1}^{n} z_{k} b_{k} \exp(-\alpha_{kj} \tau_{kj})} \right) \right]$$
(33)



$$v_{\text{corr}} = v_{\text{EOS}} + c_{\text{m}} - \delta_{\text{cm}} \left(\frac{0.35}{0.35 + d_{\text{m}}} \right)$$
 (38)

where (Abudour et al. 2013):

$$c_{\rm m} = \left(\frac{RT_{\rm cm}}{p_{\rm cm}}\right) \left(c_{\rm 1m} - \left(0.004 + c_{\rm 1m}\right) e^{-2d_{\rm m}}\right) \tag{39}$$

$$c_{1m} = \sum_{i=1}^{n} z_i c_{1i} \tag{40}$$

$$d_{\rm m} = \frac{1}{RT_{\rm cm}} \left(\frac{\partial p^{PR}}{\partial \rho}\right)_T - \left(\frac{1}{RT_{\rm cm}\rho^2}\right) \frac{a_{v1}^2}{a_{11}} \tag{41}$$

where $T_{\rm cm}$, $p_{\rm cm}$ and $\delta_{\rm cm}$ are the critical temperature, critical pressure and volume correction of the mixture at the critical point, respectively. c_{1i} is the specie-specific parameter of component i and has a linear relationship with critical compressibility ($Z_{\rm c}$) (Abudour et al. 2012b):

$$c_1 = 0.4266Z_c - 0.1101 \tag{42}$$

The term $d_{\rm m}$ can be derived using the original PR EOS (Matheis et al. 2016):

$$d_{\rm m} = \frac{v^2}{RT_{\rm cm}} \left[\frac{RT}{(v-b)^2} - \frac{2a(v+b)}{(-b^2 + 2bv + v^2)^2} \right]$$
(43)

The volume correction of the given mixture at the critical point, δ_{cm} , can be determined by (Abudour et al. 2013):

$$\delta_{\rm cm} = 0.3074 \frac{RT_{\rm cm}}{p_{\rm cm}} - \sum_{i=1}^{n} \theta_i v_{ci}$$
 (44)

where v_{ci} is the critical volume of component i; θ_i is the surface fraction of component i defined by (Abudour et al. 2013):

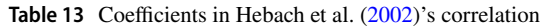
$$\theta_i = \frac{z_i v_{ci}^{2/3}}{\sum_{i=1}^n z_i v_{ci}^{2/3}} \tag{45}$$

The critical temperature of the mixture can be calculated via the following mixing rule (Abudour et al. 2013).

$$T_{\rm cm} = \sum_{i=1}^{n} \theta_i T_{\rm ci} \tag{46}$$

The critical pressure of the mixture can be determined by the correlation proposed by Aalto et al. (1996):

$$p_{\rm cm} = \frac{\left(0.2905 - 0.085\omega_{\rm m}\right)RT_{\rm cm}}{\sum_{i=1}^{n} \theta_i v_{\rm ci}}$$
(47)



Coefficients	Original value	Refitted value	
b_0 , g/(cm ³ K)	$p_0, g/(cm^3 K)$ 0.00022		
b_1	-1.9085	-1.9085	
k_0 , mN/m	27.514	25.6836	
k_1 , cm ⁶ /g ²	-35.25	-218.4717	
k_2 , cm ¹² /g ⁴	31.916	9.3192	
k_3 , cm ¹⁸ /g ⁶	-91.016	-0.9621	
k_4 , cm ³ /g	103.233	33.4068	
k ₅ , mN/m	4.513	14.4970	
k_6 , g^2/cm^6	351.903	10.9290	

where $\omega_{\rm m}$ is the acentric factor of the mixture (Abudour et al. 2013):

$$\omega_{\rm m} = \sum_{i=1}^{n} z_i \omega_i \tag{48}$$

where ω_i is the acentric factor of component *i*.

Appendix E: Summary of existing IFT correlations for CO₂/H₂O mixtures

Parachor model (Sugden 1930) can be expressed as below (Schechter and Guo 1998):

$$\sigma = \left[\sum_{i=1}^{n} P_i \left(x_i \rho_{\mathcal{L}}^{\mathcal{M}} - y_i \rho_{\mathcal{V}}^{\mathcal{M}}\right)\right]^4 \tag{49}$$

where x_i and y_i are the mole fractions of component i in liquid and vapor phases, respectively; P_i is the Parachor value of component i ($P_{\text{H}_2\text{O}} = 52$, $P_{\text{CO}_2} = 78$) (Liu et al. 2016); $\rho_{\text{L}}^{\text{M}}$ is the molar density of liquid phase in mol/cm³; $\rho_{\text{V}}^{\text{M}}$ is the molar density of vapor phase in mol/cm³.

Hebach et al. (2002)'s correlation can be expressed as:

$$\sigma = k_0 \left(1 - \exp\left(k_1 \sqrt{dd}\right) \right) + k_2 \cdot dd + k_3 \cdot dd^2 + k_4 \cdot dd^3 + k_5 \exp\left(k_6 (dd - 0.9958)\right)$$
(50)

where (Hebach et al. 2002):

$$dd = \left(\rho_{\rm H_2O} - \rho_{\rm corr}\right)^2 \tag{51}$$

$$\rho_{\text{corr}} = \begin{cases} \frac{\rho_{\text{CO}_2} + b_0 (304 - T)(10 \times p)^{b_1}}{1000} & 0.025 \text{ g/cm}^3 < \rho_{\text{CO}_2} < 0.25 \text{ g/cm}^3 \\ \rho_{\text{CO}_2} & \text{in other cases} \end{cases}$$
(52)



where $\rho_{\rm CO_2}$ is the CO₂-rich-phase density in g/cm³; $\rho_{\rm H_2O}$ is the aqueous-phase density in g/cm³; k_0 to k_6 and b_0 to b_1 are empirical coefficients. The units of T, p, and dd are K, bar, and $\rm g^2/cm^6$, respectively. Table 13 lists the values of original and refitted coefficients.

Chen and Yang (2019)'s correlation is given as:

$$\sigma = C_1 + (C_2 p_r + C_3) \ln K_{CO_2} + (C_4 p_r + C_5) \ln K_{H,O}$$
 (53)

where σ is IFT in mN/m; p_r is the reduced pressure of CO₂; C_1 to C_5 are empirical coefficients. To make fair comparisons, we refit these coefficients based on the IFT database employed in this study. Table 14 summarizes the values of these refitted coefficients.

Appendix F: Pressure-temperature coverage of phase-density and IFT data collected from the literature.

Figure 8 depicts the pressure–temperature coverage of phase-density and IFT data collected from the literature over 278–478.35 K and 2.5–1291.1 bar, and 278.15–477.59 K and 1–1200.96 bar, respectively.

Appendix G: Experimental data selection in IFT database employed in this study

The collected IFT data are further screened to remove any obvious outliers. Figure 9 shows the identification of the outliers from the collected data over 40–60 bar and 278.15–298.15 K, while Fig. 10 shows the identification of outliers from the collected data over 100–270 bar and 307.15–314.15 K.

As seen in Fig. 9a, the measured IFT data by Chun and Wilkinson (1995) and Park et al. (2005) fall into the range of 5–8 mN/m over 278.15–288.15 K and 40–60 bar, which are significantly lower than the measured IFT data (i.e., around 22–28 mN/m) obtained by other studies under similar conditions. Figure 9b indicates that the measured IFT data by Chun and Wilkinson (1995) and Park et al. (2005) fall into the range of 10–14 mN/m over 293.15–298.15 K and 50–70 bar, which are significantly lower than the measured

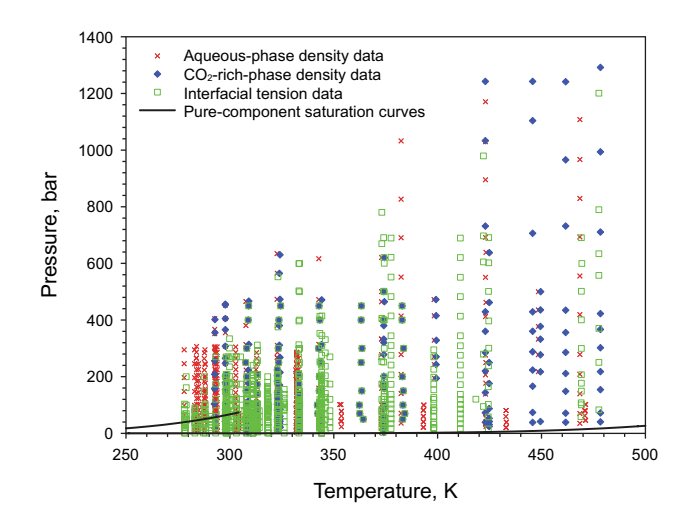


Fig. 8 Pressure–temperature coverage of phase-density and IFT data collected from the literature. The solid curves stand for pure-CO₂ (left) and pure-H₂O (right) saturation curves, respectively

IFT data (i.e., around 28–31 mN/m) obtained by other studies under similar conditions.

Figure 10 indicates that the measured data by Bachu and Bennion (2009) fall into the range of 16–19 mN/m over 307.15–314.15 K and 120–270 bar, which are significantly lower than the measured IFT values (i.e., around 30 mN/m) obtained by other studies under similar conditions. No outlier exists at other temperature and pressure conditions. We have removed these outliers in the IFT regression analysis.

Appendix H: Derivation of activity coefficient in the fugacity expression when Huron-Vidal mixing rule is used.

Similar to the approach used by Wong and Sandler (1992), the activity coefficient of component i can be expressed by the following formula:

$$\ln \gamma_i = \frac{1}{RT} \frac{\partial G_{\infty}^{E}}{\partial z_i} \tag{54}$$

where the excess Gibbs free energy can be expressed as (Huron and Vidal 1979):

 Table 14 Refitted coefficients in Chen and Yang's correlation

Coefficient set	Pressure range	C_1	C_2	C_3	C_4	C_5
1	Full	-64.7356	2.3405	16.3306	2.0919	-7.1593
2	$p \le 73.8$ bar	-34.3182	6.5500	10.8716	7.9611	-7.9076
	Else	-49.7215	0.2460	18.0648	0.1813	-1.9879



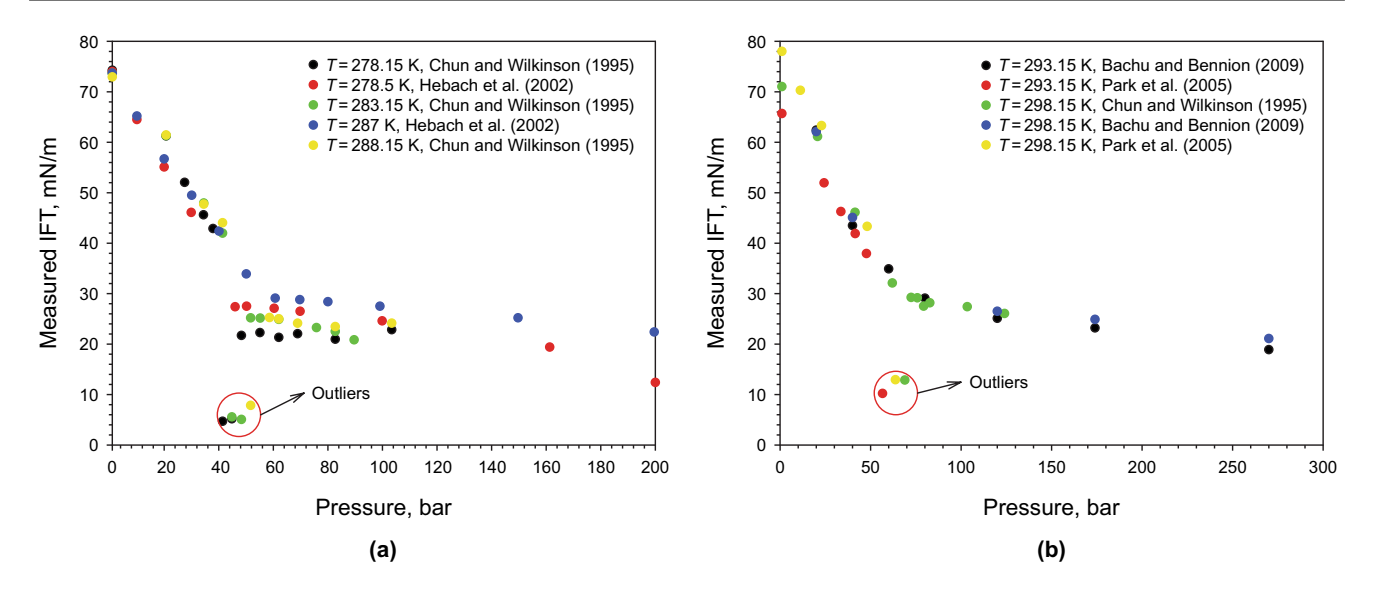


Fig. 9 Identification of the outliers at T = 278.15 - 288.15 K (a) and T = 293.15 - 298.15 K (b). Outliers are from the studies by Chun and Wilkinson (1995) and Park et al. (2005)

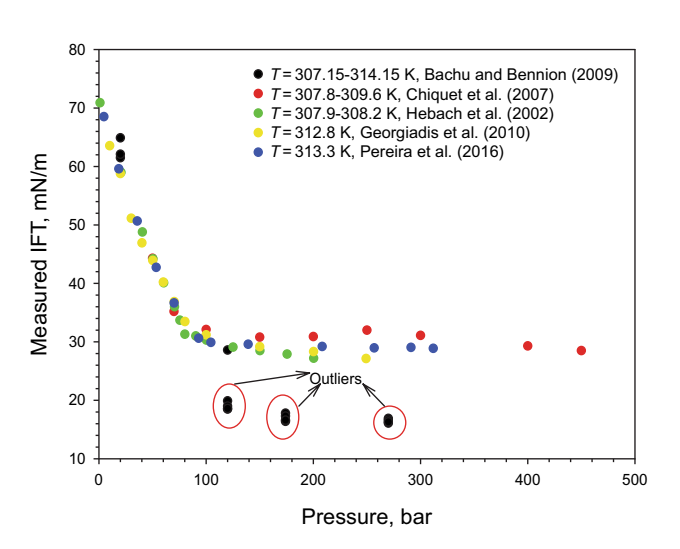


Fig. 10 Identification of the outliers at moderate temperature (307.15–314.15 K) conditions. Outliers are from the study by Bachu and Bennion (2009)

$$G_{\infty}^{E} = RT \sum_{i=1}^{n} z_{i} \frac{\sum_{j=1}^{n} \tau_{ji} b_{j} z_{j} \exp(-\alpha_{ji} \tau_{ji})}{\sum_{k=1}^{n} b_{k} z_{k} \exp(-\alpha_{ki} \tau_{ki})}$$
(55)

To make the derivation process more intuitive, we can set i=1 (the first component) and n=2 (two compounds in the system). Then the excess Gibbs free energy can be expressed as:

$$\frac{G_{\infty}^{E}}{RT} = z_{1} \cdot \frac{\sum_{j=1}^{n} \tau_{j1} b_{j} z_{j} \exp(-\alpha_{j1} \tau_{j1})}{\sum_{k=1}^{n} b_{k} z_{k} \exp(-\alpha_{k1} \tau_{k1})} + z_{2} \cdot \frac{\sum_{j=1}^{n} \tau_{j2} b_{j} z_{j} \exp(-\alpha_{j2} \tau_{j2})}{\sum_{k=1}^{n} b_{k} z_{k} \exp(-\alpha_{k2} \tau_{k2})}$$
(56)

Taking the partial derivative of the first term in the right hand side of Eq. (56) yields:

$$\frac{\partial}{\partial z_{1}} \left(z_{1} \cdot \frac{\sum_{j=1}^{n} \tau_{j1} b_{j} z_{j} \exp(-\alpha_{j1} \tau_{j1})}{\sum_{k=1}^{n} b_{k} z_{k} \exp(-\alpha_{k1} \tau_{k1})} \right) \\
= \frac{\sum_{j=1}^{n} \tau_{j1} b_{j} z_{j} \exp(-\alpha_{j1} \tau_{j1})}{\sum_{k=1}^{n} b_{k} z_{k} \exp(-\alpha_{k1} \tau_{k1})} + z_{1} \\
\cdot \left(\frac{\tau_{11} b_{1} \exp(-\alpha_{11} \tau_{11}) \cdot \left(\sum_{k=1}^{n} b_{k} z_{k} \exp(-\alpha_{k1} \tau_{k1})\right)}{\left(\sum_{k=1}^{n} b_{k} z_{k} \exp(-\alpha_{k1} \tau_{k1})\right)^{2}} - \frac{b_{1} \exp(-\alpha_{11} \tau_{11}) \cdot \left(\sum_{j=1}^{n} \tau_{j1} b_{j} z_{j} \exp(-\alpha_{j1} \tau_{j1})\right)}{\left(\sum_{k=1}^{n} b_{k} z_{k} \exp(-\alpha_{k1} \tau_{k1})\right)^{2}} \right)$$
(57)



Taking the partial derivative of the second term in the right hand side of Eq. (56) yields:

$$\frac{\partial}{\partial z_{1}} \left(z_{2} \cdot \frac{\sum_{j=1}^{n} \tau_{j2} b_{j} z_{j} \exp(-\alpha_{j2} \tau_{j2})}{\sum_{k=1}^{n} b_{k} z_{k} \exp(-\alpha_{k2} \tau_{k2})} \right)$$

$$= z_{2} \cdot \left(\frac{\tau_{12} b_{1} \exp(-\alpha_{12} \tau_{12}) \cdot \left(\sum_{k=1}^{n} b_{k} z_{k} \exp(-\alpha_{k2} \tau_{k2})\right)}{\left(\sum_{k=1}^{n} b_{k} z_{k} \exp(-\alpha_{k2} \tau_{k2})\right)^{2}} - \frac{b_{1} \exp(-\alpha_{12} \tau_{12}) \cdot \left(\sum_{j=1}^{n} \tau_{j2} b_{j} z_{j} \exp(-\alpha_{j2} \tau_{j2})\right)}{\left(\sum_{k=1}^{n} b_{k} z_{k} \exp(-\alpha_{k2} \tau_{k2})\right)^{2}} \right) (58)$$

As such, Eq. (54) can be expressed as:

$$\frac{1}{RT} \frac{\partial G_{\infty}^{E}}{\partial z_{1}} = \frac{\sum_{j=1}^{n} \tau_{j1} b_{j} z_{j} \exp(-\alpha_{j1} \tau_{j1})}{\sum_{k=1}^{n} b_{k} z_{k} \exp(-\alpha_{k1} \tau_{k1})} + \frac{z_{1} b_{1} \exp(-\alpha_{11} \tau_{11})}{\sum_{k=1}^{n} b_{k} z_{k} \exp(-\alpha_{k1} \tau_{k1})} \cdot \left(\tau_{11} - \frac{\sum_{j=1}^{n} \tau_{j1} b_{j} z_{j} \exp(-\alpha_{j1} \tau_{j1})}{\sum_{k=1}^{n} b_{k} z_{k} \exp(-\alpha_{k1} \tau_{k1})}\right) + \frac{z_{2} b_{1} \exp(-\alpha_{12} \tau_{12})}{\sum_{k=1}^{n} b_{k} z_{k} \exp(-\alpha_{k2} \tau_{k2})} \cdot \left(\tau_{12} - \frac{\sum_{j=1}^{n} \tau_{j2} b_{j} z_{j} \exp(-\alpha_{j2} \tau_{j2})}{\sum_{k=1}^{n} b_{k} z_{k} \exp(-\alpha_{k2} \tau_{k2})}\right)$$
(59)

Using letter *i* to replace number 1 leads to a general expression of activity coefficient (Huron and Vidal 1979):

$$\begin{split} & \ln \gamma_i = \frac{1}{RT} \frac{\partial G_{\infty}^{\mathbf{E}}}{\partial z_i} \\ & = \frac{\sum_{j=1}^n \tau_{ji} b_j z_j \exp\left(-\alpha_{ji} \tau_{ji}\right)}{\sum_{k=1}^n b_k z_k \exp\left(-\alpha_{ki} \tau_{ki}\right)} \\ & + \sum_{j=1}^n \left[\frac{b_i z_j \exp\left(-\alpha_{ij} \tau_{ij}\right)}{\sum_{k=1}^n b_k z_k \exp\left(-\alpha_{kj} \tau_{kj}\right)} \left(\tau_{ij} - \frac{\sum_{l=1}^n \tau_{lj} b_l z_l \exp\left(-\alpha_{lj} \tau_{lj}\right)}{\sum_{k=1}^n b_k z_k \exp\left(-\alpha_{kj} \tau_{kj}\right)} \right) \right] \end{split}$$

$$(60)$$

References

- Aalto M, Keskinen KI, Aittamaa J, Liukkonen S. An improved correlation for compressed liquid densities of hydrocarbons. Part 2. Mixtures. Fluid Phase Equilib. 1996;114:21–35. https://doi.org/10.1016/0378-3812(95)02824-2.
- Aasen A, Hammer M, Skaugen G, Jakobsen JP, Wilhelmsen Ø. Thermodynamic models to accurately describe the PVTxybehavior of water/carbon dioxide mixtures. Fluid Phase Equilib. 2017;442:125–39. https://doi.org/10.1016/j.fluid.2017.02.006.
- Abudour AM, Mohammad SA, Gasem KAM. Modeling high-pressure phase equilibria of coalbed gases/water mixtures with the Peng–Robinson equation of state. Fluid Phase Equilib. 2012;319:77–89. https://doi.org/10.1016/j.fluid.2012.01.030.
- Abudour AM, Mohammad SA, Robinson R, Gasem KAM. Volumetranslated Peng-Robinson equation of state for saturated and

- single-phase liquid densities. Fluid Phase Equilib. 2012;335:74–87. https://doi.org/10.1016/j.ijrefrig.2019.04.014.
- Abudour AM, Mohammad SA, Robinson RL, Gasem KAM. Volumetranslated Peng–Robinson equation of state for liquid densities of diverse binary mixtures. Fluid Phase Equilib. 2013;349:37–55. https://doi.org/10.1016/j.fluid.2013.04.002.
- Akutsu T, Yamaji Y, Yamaguchi H, Watanabe M, Smith R, Inomata H. Interfacial tension between water and high pressure CO₂ in the presence of hydrocarbon surfactants. Fluid Phase Equilib. 2007;257:163–8. https://doi.org/10.1016/j.fluid.2007.01.040.
- Bachu S, Bennion DB. Interfacial tension between CO₂, freshwater, and brine in the range of pressure from (2 to 27) MPa, temperature from (20 to 125) °C, and water salinity from (0 to 334000) mg·L⁻¹. J Chem Eng Data. 2009;54:765–75. https://doi.org/10.1021/je800529x.
- Bikkina PK, Shoham O, Uppaluri R. Equilibrated interfacial tension data of the CO₂-water system at high pressures and moderate temperatures. J Chem Eng Data. 2011;56:3725–33. https://doi.org/10.1021/je200302h.
- Briones JA, Mullins JC, Thies MC. Ternary phase equilibria for acetic acid-water mixtures with supercritical carbon dioxide. Fluid Phase Equilib. 1987;36:235–46. https://doi.org/10.1016/0378-3812(87)85026-4.
- Chalbaud C, Robin M, Lombard JM, Martin F, Egermann P, Bertin H. Interfacial tension measurements and wettability evaluation for geological CO₂ storage. Adv Water Resour. 2009;32:98–109. https://doi.org/10.1016/j.advwatres.2008.10.012.
- Chen Z, Yang D. Correlations/estimation of equilibrium interfacial tension for methane/CO₂-water/brine systems based on mutual solubility. Fluid Phase Equilib. 2019;483:197–208. https://doi.org/10.1016/j.fluid.2018.11.037.
- Chiquet P, Daridon J, Broseta D, Thibeau S. CO₂/water interfacial tensions under pressure and temperature conditions of CO₂ geological storage. Energy Conversat Manag. 2007;48:736–44. https://doi.org/10.1016/j.enconman.2006.09.011.
- Chun BS, Wilkinson GT. Interfacial tension in high-pressure carbon dioxide mixtures. Ind Eng Chem Res. 1995;34:4371–7. https://doi.org/10.1021/ie00039a029.
- Dalmolin I, Skovroinski E, Biasi A, Corazza M, Dariva C, Oliverira JV. Solubility of carbon dioxide in binary and ternary mixtures with ethanol and water. Fluid Phase Equilib. 2006;245:193–200. https://doi.org/10.1016/j.fluid.2006.04.017.
- Da Rocha SRP, Harrison KL, Johnston KP. Effect of surfactants on the interfacial tension and emulsion formation between water and carbon dioxide. Langmuir. 1999;15:419–28. https://doi.org/10.1021/ la980844k.
- Dohrn R, Bünz AP, Devlieghere F, Thelen D. Experimental measurements of phase equilibria for ternary and quaternary systems of glucose, water, CO₂ and ethanol with a novel apparatus. Fluid Phase Equilib. 1993;83:149–58. https://doi.org/10.1016/0378-3812(93)87017-U.



- D'Souza R, Patrick JR, Teja AS. High pressure phase equilibria in the carbon dioxide—*n*-hexadecane and carbon dioxide-water systems. Can J Chem Eng. 1988;66:319–23. https://doi.org/10.1002/cjce.5450660221.
- Efika EC, Hoballah R, Li X, May EF, Nania M, Vicente YS, Trusler JPM. Saturated phase densities of (CO₂ + H₂O) at temperatures from (293 to 450) K and pressures up to 64 MPa. J Chem Thermodyn. 2016;93:347–59. https://doi.org/10.1016/j.jct.2015.06.034.
- Gasem KAM, Gao W, Pan Z, Robinson RL. A modified temperature dependence for the Peng–Robinson equation of state. Fluid Phase Equilib. 2001;181:113–25. https://doi.org/10.1016/S0378-3812(01)00488-5.
- Georgiadis A, Maitland G, Trusler JP, Bismarck A. Interfacial tension measurements of the (H₂O + CO₂) system at elevated pressures and temperatures. J Chem Eng Data. 2010;55:4168–75. https://doi.org/10.1021/je100198g.
- Gernert J, Span R. EOS-CG: a Helmholtz energy mixture model for humid gases and CCS mixtures. J Chem Thermodyn. 2016;93:274–93. https://doi.org/10.1016/j.jct.2015.05.015.
- Gillepsie PC, Wilson GM. Vapor-liquid and liquid–liquid equilibria: water-methane, water-carbon dioxide, water-hydrogen sulfide, water-n-pentane, water-methane-n-pentane. Tulsa.: Gas Processors Association; 1982.
- Guo H, Chen Y, Hu Q, Lu W, Ou W. Quantitative Raman spectroscopic investigation of geo-fluids high-pressure phase equilibria: part I. Accurate calibration and determination of CO₂ solubility in water from 273.15 to 573.15 K and from 10 to 120 MPa. Fluid Phase Equilib. 2014;382:70–9. https://doi.org/10.1016/j.fluid.2014.08.032.
- Han JN, Shin HY, Min BM, Han KH, Cho A. Measurement and correlation of high-pressure phase behavior of carbon dioxide + water system. J Ind Eng Chem. 2009;15:212–6. https://doi. org/10.1016/j.jiec.2008.09.012.
- Hebach A, Oberhof A, Dahmen N, Kögel A, Ederer H, Dinjus E. Interfacial tension at elevated pressures—measurements and correlations in the water + carbon dioxide system. J Chem Eng Data. 2002;47:1540–6. https://doi.org/10.1021/je025569p.
- Hebach A, Oberhof A, Dahmen N. Density of water plus carbon dioxide at elevated pressures: measurements and correlation. J Chem Eng Data. 2004;49:950–3. https://doi.org/10.1021/je034260i.
- Heuer GJ. Interfacial tension of water against hydrocarbons and other gases and adsorption of methane on solids at reservoir temperatures and pressures. PhD Dissertation, Univ. of Texas at Austin, Austin, Texas; 1957.
- Hough EW, Henuer GJ, Walker JW. An improved pendant drop, interfacial tension apparatus and data for carbon dioxide and water. Pet Trans AIME. 1959;216:469–72.
- Huron MJ, Vidal J. New mixing rules in simple equations of state for representing vapor-liquid equilibria of strongly nonideal mixtures. Fluid Phase Equilib. 1979;3:255–71. https://doi.org/10.1016/0378-3812(79)80001-1.
- Japkowicz N, Shah M. Evaluating learning algorithms—a classification perspective. Cambridge: Cambridge University Press; 2011. https://doi.org/10.1017/CBO9780511921803.
- Jhaveri BS, Youngren GK. Three-parameter modification of the Peng–Robinson equation of state to improve volumetric predictions. SPE Res Eng. 1988;8:1033–40. https://doi.org/10.2118/13118-PA.
- Khosharay S, Varaminian F. Experimental and modeling investigation on surface tension and surface properties of (CH₄ + H₂O), (C₂H₆ + H₂O), (CO₂ + H₂O) and (C₃H₈ + H₂O) from 284.15 K to 312.15 K and pressures up to 60 bar. Int J Refrig. 2014;47:26–35. https://doi.org/10.1016/j.ijrefrig.2014.08.003.
- King MB, Mubarak A, Kim JD, Bott TR. The mutual solubilities of water with supercritical and liquid carbon-dioxide. J Supercrit Fluids. 1992;5:296–302. https://doi.org/10.1016/0896-8446(92)90021-B.

- Kontogeorgis GM, Voutsas EC, Yakoumis IV, Tassios DP. An equation of state for associating fluids. Ind Eng Chem Res. 1996;35:4310–8. https://doi.org/10.1021/ie9600203.
- Kvamme B, Kuznetsova T, Hebach A, Oberhof A, Lunde E. Measurements and modelling of interfacial tension for water + carbon dioxide systems at elevated pressures. Comput Mater Sci. 2007;38:506–13. https://doi.org/10.1016/j.commatsci.2006.01.020.
- Kunz O, Wagner W. The GERG-2008 wide-range equation of state for natural gases and other mixtures: an expansion of GERG-2004. J Chem Eng Data. 2012;57:3032–91. https://doi.org/10.1021/je300 655b.
- Lemmon EW, McLinden MO, Friend DG. Thermophysical properties of fluid systems. In: Linstrom PJ, Mallard WG, editors. NIST chemistry WebBook, NIST standard reference database number 69. Gaithersburg: National Institute of Standards and Technology; 2011, p. 20899 https://doi.org/10.18434/T4D303
- Li R, Li H. Improved three-phase equilibrium calculation algorithm for water/hydrocarbon mixtures. Fuel. 2019;244:517–27. https:// doi.org/10.1016/j.fuel.2019.02.026.
- Li Z, Dong M, Li S, Dai L. Densities and solubilities for binary systems of carbon dioxide plus water and carbon dioxide plus brine at 59 °C and pressures to 29 MPa. J Chem Eng Data. 2004;49:1026–31. https://doi.org/10.1021/je049945c.
- Liu Y, Li H, Okuno R. Measurements and modeling of interfacial tension for CO₂/CH₄/brine systems under reservoir conditions. Ind Eng Chem Res. 2016;55:12358–75. https://doi.org/10.1021/acs.jecr.6b02446.
- Martin JJ. Cubic equations of state—which? Ind Eng Chem Fundam. 1979;18:81–97. https://doi.org/10.1021/i160070a001.
- Martinez A, Guennec YL, Privat R, Jaubert JN, Mathias PM. Analysis of the combinations of property data that are suitable for a safe estimation of consistent Twu α-function parameters: updated parameter values for the translated-consistent tc-PR and tc-RK cubic equation of state. J Chem Eng Data. 2018;3:3980–8. https://doi.org/10.1021/acs.jced.8b00640.
- Matheis J, Müller H, Lenz C, Pfitzner M, Hickel S. Volume translation methods for real-gas computational fluid dynamics simulations. J Supercrit Fluids. 2016;107:422–32. https://doi.org/10.1016/j. supflu.2015.10.004.
- Mathias PM, Copeman TW. Extension of the Peng–Robinson equation of state to complex mixtures: evaluation of the various forms of the local composition concept. Fluid Phase Equilib. 1983;13:91–108. https://doi.org/10.1016/0378-3812(83)80084-3.
- Mathias PM, Naheiri T, Oh EM. A density correction for the Peng–Robinson equation of state. Fluid Phase Equilib. 1989;47:77–87. https://doi.org/10.1016/0378-3812(89)80051-2.
- Michelsen ML, Mollerup JM. Thermodynamic models: fundamentals & computational aspects. 2nd ed. Holte: Tie-Line Publications; 2007.
- Nighswander JA, Kalogerakis N, Mehrotra AK. Solubilities of carbon dioxide in water and 1 wt% NaCl solution at pressures up to 10 MPa and temperatures from 80 to 200 °C. J Chem Eng Data. 1989;34:355–60. https://doi.org/10.1021/je00057a027.
- Park JY, Lim JS, Yoon CH, Lee CH, Park KP. Effect of a fluorinated sodium bis(2-ethylhexyl) sulfosuccinate (Aerosol-OT, AOT) analogue surfactant on the interfacial tension of CO₂ + water and CO₂ + Ni-plating solution in near- and supercritical CO₂. J Chem Eng Data. 2005;50:299–308. https://doi.org/10.1021/je0499667.
- Pedersen KS, Christensen PL, Shaikh JA. Phase behavior of petroleum reservoir fluids. Boca Raton: CRC Press; 2014. https://doi. org/10.1201/b17887.
- Peneloux A, Rauzy E, Freze R. A consistent correction for Redlich–Kwong–Soave volumes. Fluid Phase Equilib. 1982;8:7–23. https://doi.org/10.1016/0378-3812(82)80002-2.



- Peng DY, Robinson DB. A new two-constant equation of state. Ind Eng Chem Fundam. 1976;15:59–64. https://doi.org/10.1021/i160057a011.
- Pereira L, Chapoy A, Burgass R, Oliveira MB, Coutinho J, Tohidi B. Study of the impact of high temperatures and pressures on the equilibrium densities and interfacial tension of the carbon dioxide/ water system. J Chem Thernodyn. 2016;93:404–15. https://doi. org/10.1016/j.jct.2015.05.005.
- Sako T, Sugata T, Nakazawa N, Obuko T, Sato M, Taguchi T, Hiaki T. Phase equilibrium study of extraction and concentration of furfural produced in reactor using supercritical carbon dioxide. J Chem Eng Jpn. 1991;24:449–54. https://doi.org/10.1252/ jcej.24.449.
- Schechter DS, Guo B. Parachor based on modern physics and their uses in IFT prediction of reservoir fluids. SPE Res Eval Eng. 1998;1:207–17. https://doi.org/10.2118/30785-PA.
- Shariat A, Moore RG, Mehta SA, Fraassen KC, Newsham KE, Rushing JA. Laboratory measurements of CO₂–H₂O interfacial tension at HP/HT conditions: implications for CO₂ sequestration in deep aquifers. In: Carbon management technology conference, 7–9 Februrary, Orlando, Florida, USA; 2012. https://doi.org/10.7122/150010-MS
- Soave G. Equilibrium constants from a modified Redlich–Kwong equation of state. Chem Eng Sci. 1972;27:1197–203. https://doi.org/10.1016/0009-2509(72)80096-4.
- Song KY, Kobayashi R. Water content of CO₂ in equilibrium with liquid water and/or hydrates. SPE Form Eval. 1987;2:500–8. https://doi.org/10.2118/15905-PA.
- Spycher N, Pruess K, King JE. CO₂–H₂O mixtures in the geological sequestration of CO₂. I. Assessment and calculation of mutual solubilities from 12 to 100° and up to 600 bar. Geochim Cosmochim Acta. 2003;67:3015–31. https://doi.org/10.1016/S0016-7037(03)00273-4.
- Stryjek R, Vera JH. PRSV: an improved Peng–Robinson equation of state for pure compounds and mixtures. Can J Chem Eng. 1986;64:323–33. https://doi.org/10.1002/cjce.5450640224.
- Sugden S. The Parachors and valency. London: G. Routledge; 1930.
 Tabasinejad F, Barzin Y, Moore GR, Mehta SA, Fraassen KCV, Rushing JA, Newsham KE. Water/CO₂ system at high pressure and temperature conditions: measurement and modeling of density in equilibrium liquid and vapor phases. In: SPE EUROPEC/EAGE annual conference and exhibition, 14–17 June, Barcelona, Spain;
- Teng H, Yamasaki A, Chun MK, Lee H. Solubility of liquid CO_2 in water at temperatures from 278 K to 293 K and pressures from 6.44 MPa to 29.49 MPa and densities of the corresponding aqueous solutions. J Chem Thermodyn. 1997;29:1301–10. https://doi.org/10.1006/jcht.1997.0249.

2010. https://doi.org/10.2118/131636-MS.

Tödheide K, Frank EU. Das Zweiphasengebiet und die kritische Kurve im system Kohlendioxid-Wasser bis zu Drucken von 3500 bar. Z Phys Chem. 1962;37:387-401. https://doi.org/10.1524/ZPCH.1963.37.5_6.387.

- Trusler JPM. Thermophysical properties and phase behavior of fluids for application in carbon capture and storage processes. Ann Rev Chem Biomol Eng. 2017;8:381–402. https://doi.org/10.1146/annurev-chembioeng-060816-101426.
- Twu CH, Bluck D, Cunningham JR, Coon JE. A cubic equation of state with a new alpha function and a new mixing rule. Fluid Phase Equilib. 1991;69:33–50. https://doi.org/10.1016/0378-3812(91)90024-2.
- Valtz A, Chaopy A, Coquelet C, Paricaud P, Richon D. Vapor-liquid equilibria in the carbon dioxide-water system, measurement and modeling from 278.2 to 318.2 K. Fluid Phase Equilib. 2004;226:333–44. https://doi.org/10.1016/j.fluid.2004.10.013.
- van der Waals JD. Continuity of the gaseous and liquid state of matter. PhD Dissertation, Univ. of Leiden; 1873.
- Weibe R, Gaddy VL. The solubility in water of carbon dioxide at 50, 75, and 100 °C, at pressures to 700 atmospheres. J Am Chem Soc. 1939;61:315–8. https://doi.org/10.1021/ja01871a025.
- Weibe R, Gaddy VL. The solubility of carbon dioxide in water at various temperatures from 12 to 40 °C and at pressures to 500 atmospheres: critical phenomena. J Am Chem Soc. 1940;62:815–7. https://doi.org/10.1021/ja01861a033.
- Wong DSH, Sandler SI. A theoretically correct mixing rule for cubic equations of state. AIChE J. 1992;38:671–80. https://doi. org/10.1002/aic.690380505.
- Yaginuma R, Sato Y, Kodama D, Tanaka H, Kato M. Saturated densities of carbon dioxide + water mixture at 304.1 K and pressures to 10 MPa. J Jpn Inst Energy. 2000;79:144–6. https://doi.org/10.3775/jie.79.144.
- Young AF, Pessoa FLP, Ahón VRR. Comparison of 20 alpha functions applied in the Peng–Robinson equation of state for vapor pressure estimation. Ind Eng Chem Res. 2016;55:6506–16. https://doi.org/10.1021/acs.iecr.6b00721.
- Young AF, Pessoa FLP, Ahón VRR. Comparison of volume translation and co-volume functions applied in the Peng–Robinson EOS for volumetric corrections. Fluid Phase Equilib. 2017;435:73–87. https://doi.org/10.1016/j.fluid.2016.12.016.
- Zhang J, Feng Q, Wang S, Zhang X, Wang S. Estimation of CO₂-brine interfacial tension using an artificial neural network. J Supercrit Fluids. 2016;107:31–7. https://doi.org/10.1016/j.supflu.2015.08.010.
- Zhao H, Fedkin MV, Dilmore RM, Lvov SN. Carbon dioxide solubility in aqueous solutions of sodium chloride at geological conditions: experimental results at 323.15, 373.15, and 423.15 K and 150 bar and modeling up to 573.15 K and 2000 bar. Geochim Cosmochim Acta. 2015;149:165–89. https://doi.org/10.1016/j.gca.2014.11.004.
- Zhao H, Lvov SN. Phase behavior of the CO₂–H₂O system at temperatures of 273–623 K and pressures of 0.1–200 MPa using Peng–Robinson–Stryjek–Vera equation of state with a modified Wong–Sandler mixing rule: an extension to the CO₂–CH₄–H₂O system. Fluid Phase Equilib. 2016;417:96–10. https://doi.org/10.1016/j.fluid.2016.0.027.

